In Silico Modeling of Shear-Stress-Induced Nitric Oxide Production in Endothelial Cells through Systems Biology

Andrew Koo,[†||] David Nordsletten,[¶] Renato Umeton,[‡] Beracah Yankama,[§] Shiva Ayyadurai,[†] Guillermo García-Cardeña,[||] and C. Forbes Dewey, Jr.[†‡*]

[†]Department of Biological Engineering, [‡]Department of Mechanical Engineering, and [§]Laboratory for Information and Decision Systems, Massachusetts Institute of Technology, Cambridge, Massachusetts; [¶]Department of Biomedical Engineering, King's College London, London, United Kingdom; and [||]Laboratory for Systems Biology, Center for Excellence in Vascular Biology, Department of Pathology, Brigham and Women's Hospital and Harvard Medical School, Boston, Massachusetts

ABSTRACT Nitric oxide (NO) produced by vascular endothelial cells is a potent vasodilator and an antiinflammatory mediator. Regulating production of endothelial-derived NO is a complex undertaking, involving multiple signaling and genetic pathways that are activated by diverse humoral and biomechanical stimuli. To gain a thorough understanding of the rich diversity of responses observed experimentally, it is necessary to account for an ensemble of these pathways acting simultaneously. In this article, we have assembled four quantitative molecular pathways previously proposed for shear-stress-induced NO production. In these pathways, endothelial NO synthase is activated 1), via calcium release, 2), via phosphorylation reactions, and 3), via enhanced protein expression. To these activation pathways, we have added a fourth, a pathway describing actual NO production from endothelial NO synthase and its various protein partners. These pathways were combined and simulated using CytoSolve, a computational environment for combining independent pathway calculations. The integrated model is able to describe the experimentally observed change in NO production with time after the application of fluid shear stress. This model can also be used to predict the specific effects on the system after interventional pharmacological or genetic changes. Importantly, this model reflects the up-to-date understanding of the NO system, providing a platform upon which information can be aggregated in an additive way.

INTRODUCTION

One of the most important functions of vascular endothelial cells is to produce nitric oxide (NO). This molecule has a number of different roles in vascular stasis, including acting as a potent vasodilator and a mediator of inflammation (1). Not surprisingly, human vascular endothelial cells have developed multiple pathways by which production of NO is regulated by humoral and biomechnical stimuli via the expression and activation of endothelial nitric oxide synthase (eNOS). Exploring these different pathways one at a time is difficult, because the system is not separable—multiple pathways contribute to the production rate under all physiological circumstances. To understand and model the rich diversity of responses that have been observed experimentally, it is necessary to account for an ensemble of these pathways acting simultaneously over an extensive range of timescales.

The advancements of modern biology and computer science have increasingly enabled researchers to build such multipathway models. In the past two decades, experiments have been conducted that provide quantitative information between molecular species in the cell and their evolution under specific stimuli, facilitating construction of quantitative biochemical pathways that may be used as predictors of cellular response under a wider range of physiological or pathophysiological conditions. This sort of quantitative analysis of molecular pathways provides a valuable tool for assessing biological mechanisms and validating hypothetical mechanisms by comparing simulation results with experimental data.

One of the major hurdles in this process has been the development of in silico models that are sufficiently detailed to describe the complex phenomena observed. The current state of the art is to construct quantitative models based on selected subpaths within a larger molecular pathway. This process is time-consuming, requiring in-depth literature searches, experimentation, and parameter estimation. These isolated subpath models are invaluable and often provide insight into specific biochemical mechanisms. However, these subpathway models are often not independent in vivo or in vitro and have cross-sensitivities due to common species and overlapping reactions. As a result, to address more complex questions, such as the evolution of NO under mechanical shear stress, it is necessary to systematically integrate these subpaths to provide a more comprehensive and accurate purview of cellular mechanisms.

The current process of integrating multiple molecular pathways involves hand curation of individual models into a single monolithic model (see Fig. 1 *A*). Due to the use of different model coding environments, variable names,

Submitted October 23, 2012, and accepted for publication March 27, 2013.

*Correspondence: cfdewey@mit.edu

Editor: Peter Hunter

0006-3495/13/05/2295/12 $2.00

http://dx.doi.org/10.1016/j.bpj.2013.03.052

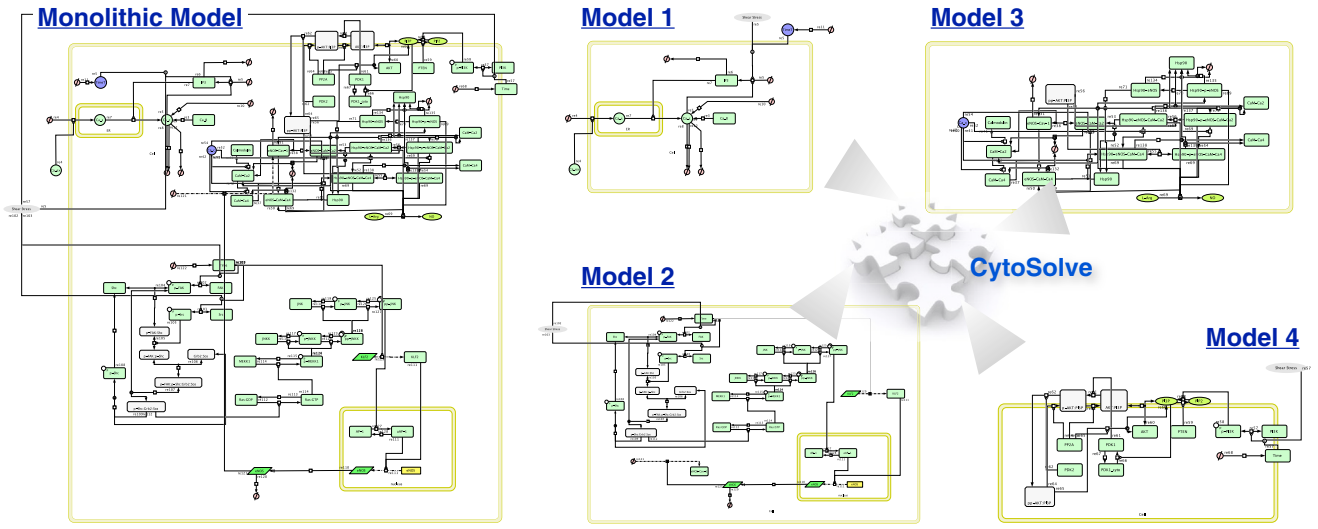

Monolithic Approach	CytoSolve Approach
• Difficult to maintain a large pathway	• Scaleable
• Many knowledge domain needed	• Encourage collaboration
• Applicable for public models only	• Applicable for both public and private models
• Models have to be in one standard format	• Models can be in multiple formats
• Models must be run on the same hardware platform in the same geological location	• Models may be resident on different hardware at different location

FIGURE 1 Comparison between the monolithic and CytoSolve approaches in building an integrated model.

pathway separation methodologies, and solution strategies, assembly of monolithic models typically requires substantial rewriting of previously published models. In this process, the links to previously published subpaths become difficult to decipher, and the manual work may be prone to errors, especially for large networks. The process of including new data elements to subpath models that more accurately detail biochemical reaction steps is also nontrivial and often burdensome. Of most importance scientifically, monolithic model integration loses much of the history and progression of pathway determination and development, particularly the detailed experimental condition on which the original models and parameters are based (2).

In this article, an alternative approach based on the binding-expression concept is adapted (see Fig. 1 *B*) and the integrated model is viewed as an ontology. Any previously published subpath model is retained in its entirety, allowing it to be updated, extracted, replaced, or removed. Subpathway models are then integrated through bindings that identify common species in and alterations made to each model due to their integration. In our work, the creation of these bindings has been semiautomated through the use of MIRIAM (3) annotations and XML standard formats such as SBML (4) that support computational parsing and reasoning. In this way, common species and reaction pathways can be identified despite variations in nomenclature or number of reactions, thus lowering the complexity bar for the human curator. These tools are made publicly available through CytoSolve (5), a web-accessible interface (http://cytosolve.mit.edu/) capable of model integration and simulation.

In the case of endothelia-derived NO, many pathway models governing its production have been previously established (see Table 1). In this article, we integrate four of these molecular pathway models (see Fig. 2) that modulate the activation of endothelial nitric oxide synthase (eNOS) by shear stress. Specifically, we focus on the calcium-stimulated binding of calmodulin to eNOS, AKT-mediated phosphorylation of eNOS, and upregulation of eNOS transcription through AP-1 and KLF2. These pathways are linked by an additional model describing interaction of eNOS with its protein partners. By integrating these models in CytoSolve, the dynamic regulation and

TABLE 1 List of main mechanisms of shear-stress-regulated eNOS activation

Main mechanisms of shear-stress-regulated eNOS activation				
Transcriptional regulation				
Key proteins	Known pathway	Note	References	Model inclusion
AP-1	Shc → Grb2-Sos → Ras → JNK → AP-1	Transient	(17,48)	eNOS expression
NFκB	Akt → IκK → NFκB	Transient (complex)	(16,49,50)	Not included
KLF2	? → MEK5 → ERK5 → MEF2 → KLF2	Long term	(23)	eNOS expression
Posttranslational regulation				
Phosphorylation				
Key kinases	Known pathway	Phosphorylation site	References	Model inclusion
Akt	PI3K → AKT	Ser-1177	(10)	eNOS phosphorylation
PKA	? → [cAMP] → PKA	Ser-635 (bovine)	(12)	Not included
AMPK	? → [AMP] → AMPK	Ser-1177	(22)	Not included
Protein partners				
Key partners	Effect on eNOS		References	Model inclusion
Caveolin-1	Inactivation		(51)	NO production
CaM	Activation, facilitate recruitment of Hsp90		(28,52)	Calcium influx, NO production
Hsp90	Activation, facilitate recruitment of Akt		(27,53)	NO production

production of NO by eNOS under both shear-stress and static (no-shear-stress) conditions can be investigated and tested. This use of the NO model illustrates the potential of the partitioned model approach and of the CytoSolve tools, which enable simulation of complex problems involving many parallel pathways that cannot be readily isolated experimentally.

METHODS

In this section, we discuss the individual well-characterized pathway models that regulate eNOS and, as a result, NO production. These models are linked to a new model describing the interactions of eNOS and its binding partners. The section concludes with a description of the tools used to bind the individual models together, creating a partitioned NO pathway model capable of describing the multiple phenomena that regulate NO production.

Mechanisms of shear-stress-induced NO production

Several key signaling pathways have been identified that modulate the activity of eNOS—the primary source of NO production in vascular endothelial cells. In this section, we introduce three pathway models that alter eNOS activation or regulate eNOS protein expression. To link these models, an additional model was constructed that describes the binding of calcium, calmodulin (CaM), heat-shock protein 90 (Hsp90), eNOS, and phosphorylated eNOS, as well as the resulting enzymatic production of NO. Parameters of individual models were optimized to fit the experimental observations (details of the model schemes, inputs, species, reactions, parameters, and parameter optimization steps are described in the Supporting Material).

Shear-stress-induced calcium influx and eNOS activation

In response to increased fluid shear stress, endothelial cells exhibit a transient increase in cytosolic free calcium (see Fig. 2 *A*). The influx of calcium is due to mechanisms such as activation of stress-sensitive calcium channels and activation of G-protein pathways (6). A calcium channel is directly activated by fluid shear stress, and this leads to intracellular calcium influx. G-protein-coupled receptors can also be activated by shear stress (7). Activated G-protein induces activity of phospholipase C and production of inositol 1,4,5-trisphosphate (IP3). IP3 binds to its receptor on the surface of the endoplasmic reticulum and promotes calcium release from this intracellular storage. The increased intracellular Ca^{2+} then rapidly binds to CaM, a calcium-binding protein that significantly upregulates the activity of eNOS. The elevated intracellular calcium level leads to increased calcium export via the sodium-calcium exchanger and reuptake in intracellular stores, making increase in intracellular Ca^{2+} a transient (~5-min) event (8).

To describe the calcium dynamics in response to shear stress, a mathematical model published by Wiesner et al. was used (8,9). This model assumes a step change in calcium influx mediated by the stress-sensitive calcium channel at the onset of shear stress (10 dynes/cm^2). The resulting concentration profile of calcium transient is shown in Fig. 3 *A*.

Shear-stress-induced AKT and eNOS phosphorylation

In addition to its regulation by calcium-dependent CaM binding, eNOS activity can also be regulated by posttranslational modifications, the most important of these being phosphorylation reactions. Some key phosphorylation sites include the activity-inducing serines 1177, 635, and 617, and activity inhibitors serine 116 and threonine 495. It is important to note that phosphorylation of serine 1177 is thought to be a key indicator of eNOS activity under shear-stress conditions (10,11). In this model, we focused solely on the phosphorylation of this particular site. The reaction of serine 1177 phosphorylation is catalyzed by several protein kinases, including AKT, PKA, and AMPK (1). The mechanism of how shear stress activates AMPK is still unclear, but shear-stress-induced AKT and PKA activation has been shown to be phosphoinositide 3-kinase (PI3K)-dependent (10,12). Phosphorylation of serine 1177 is significantly decreased when endothelial cells are treated with PI3K inhibitor, Ly294002, or transfected with dominant-negative AKT (10,13). These data suggest that the PI3K-AKT pathway plays a critical role in shear-stress-induced eNOS phosphorylation. Based on this experimental observation, it is assumed in our model that PI3K-dependent AKT activation is the main pathway responsible for eNOS phosphorylation. PI3K activation leads to production of phosphatidylinositol (3–5)-trisphosphate (PIP3). PIP3 then recruits cytosolic free AKT to the membrane, where it is phosphorylated by both PDK1 and PDK2 (see Fig. 2 *B*). Finally, phosphorylated AKT phosphorylates eNOS on serine 1177. It is important to note also that due to the lack of detailed kinetic

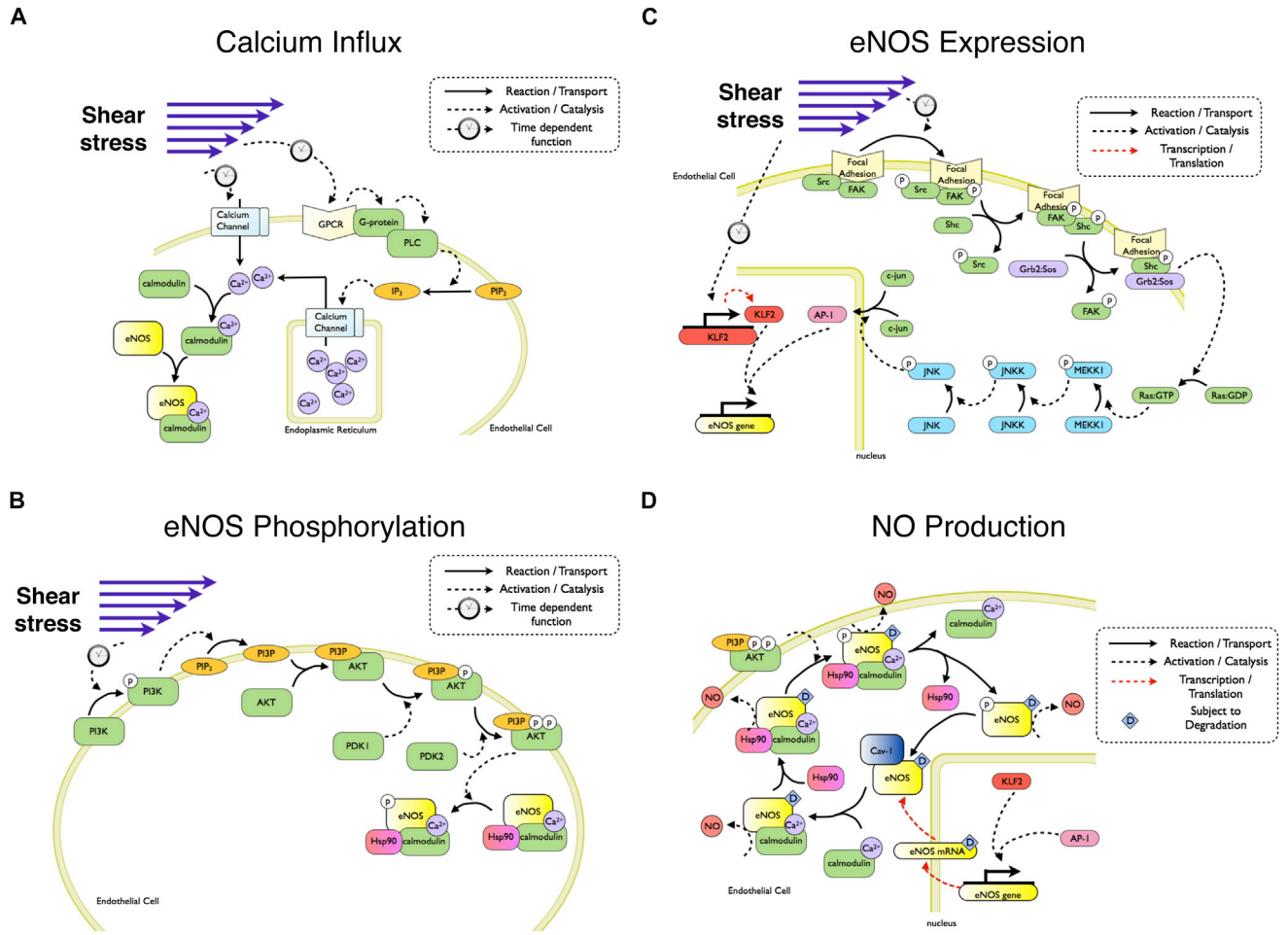

FIGURE 2 The four models of the shear-stress-induced NO production system. (*A*) The calcium influx model. (*B*) The eNOS phosphorylation model. (*C*) The eNOS expression model. (*D*) The NO production model.

parameters for the phosphorylation reactions for PKA and AMPK on serine 1177 of eNOS, the model focuses only on the AKT-dependent pathway.

The mathematical model used to describe the AKT activation process is taken from Koh et al. (14), a model originally established to study the cross talk between AKT and MAPK pathways upon binding of receptors to growth factors. This model provides a detailed illustration of the PI3K-AKT pathway, which we assumed to be conserved across different human cell types. In our model, PI3K activation was assigned to be the input signal based on a time-dependent function fit from experimental data by Go (15). Because the mechanism by which shear stress leads to activation of molecular pathways is still poorly understood, time-dependent functions were used as model inputs throughout the NO system as proxies for the mechanotransduction process (see Supporting Material for more details of the generation of time-dependent functions). In this study, laminar shear stress with a magnitude of 5 dynes/cm^2 was used in experiments. In other works used to generate model inputs for subsequent models, laminar shear stress or oscillatory shear stress with a mean magnitude of 12 dynes/cm^2 was applied. Here, we made a general assumption that eNOS activation in endothelial cells respond similarly given a shear-stress stimulus in the range 5–12 dynes/cm^2.

Shear-stress-induced eNOS expression

A third mechanism leading to an overall increase in NO production is upregulation of eNOS expression. Key transcription factors governing shear-stress-induced eNOS promoter activity include AP-1, NFκB, and KLF2 (11). The role of NFκB on eNOS expression remains controversial, as recent study indicates that expression of NFκB and eNOS is negatively correlated under shear stress (16). Therefore, in our model, we focused on simulating the effects of AP-1 and KLF2 on eNOS transcription (Fig. 2 *C*). In this model, it is assumed that there is no interaction between these two transcription factors and that they have no synergistic effect on eNOS transcription.

AP-1, a Jun-Jun homodimer or a Jun-Fos heterodimer, is involved in shear-stress-induced eNOS expression. A qualitative pathway model describing how shear stress leads to AP-1 nucleus translocation has been established previously (17). In the proposed model, shear stress activates the focal adhesion site and leads to phsophorylation of focal adhesion kinase (FAK), Src kinase, and the adaptor protein Shc. Activation of these kinases leads to formation of the first complex, FAK-Shc, then a second complex between FAK-Shc and Grb2-Sos. The second complex activates Ras protein, and initiates the MAP kinase cascade through MEKK1, JNKK, and JNK. JNK phosphorylates Jun and eventually leads to Jun dimer association to form AP-1, which translocates to nucleus and facilitates eNOS expression.

To quantitatively model the contribution of AP-1 in regulating eNOS expression, two existing mathematical models were used as the bases. The first model, excerpted from Hatakeyama et al. (18), describes the activation pathway from Src, FAK to Ras. However, since the upstream mechanical activation of Src and FAK molecules is not well understood, the kinetics of these two molecules (Fig. 3 *C*) were based on

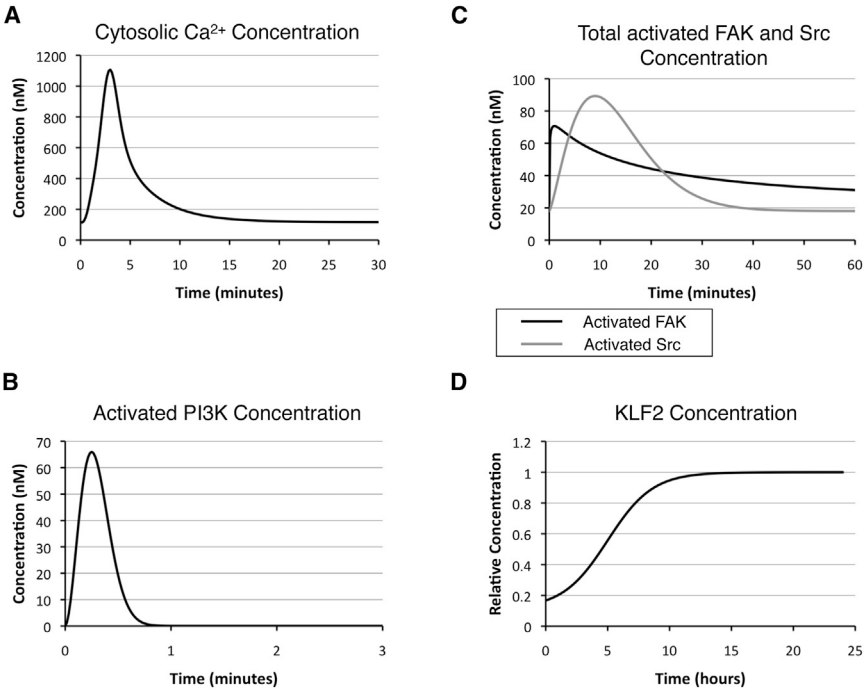

FIGURE 3 Simulation profiles of model inputs upon initiation of shear stress. The differential equations behind these simulation profiles were calculated based on time-dependent functions fit from experimental data (see Supporting Material for a detailed description of how these equations were generated). (*A*) Cytosolic Ca^{2+}. (B) Activated PI3K. (*C*) Total activated FAK and activated Src. (*D*) KLF2.

time-dependent experimental measures observed by Li et al. (19) and Jalali et al. (20). The shear-stress experiments in those two articles used a laminar shear stress of 12 dynes/cm^2. The second model, modified from the Kholodenko study (21), illustrates the kinetics of how Ras initiates the MAP kinase cascade. These two models were combined and integrated with reactions including JNK-mediated Jun phosphorylation/dimerization, AP-1 nuclear translocation, AP-1-mediated eNOS transcription, eNOS translation, and eNOS mRNA degradation. The rates of these reactions were estimated based on experimental observation and previously established models. Many parameters of this model were optimized to fit the experimental observations. Further details can be found in the Supporting Material.

KLF2, the third transcription factor responsible for eNOS expression, is characterized as leading to long-term upregulated eNOS transcription. Compared to the fast and transient nuclear translocation of AP-1 in response to shear stress, the increase in KLF2 concentration inside the nucleus is relatively slow but sustained (22). The upstream mechanosensors for KLF2 expression are still poorly understood, but its expression is known to be dependent on MEK5, ERK5, and MEF2 (23). Due to the limited amount of experimental data available to construct a complete model, KLF2 dynamics is simulated based on data from a time-course shear-stress experiment (1 Hz oscillatory shear stress of 12 $\pm$ 4 dynes/cm^2) by Young et al. (22) (Fig. 3 *D*).

Shear-stress-induced NO production

The previously described models establish the concentration profile of cytosolic free calcium, phosphorylated eNOS, and total eNOS expression in response to shear stress. However, to integrate these pathways and understand NO production, one additional model was necessary to characterize the interactions of eNOS and its binding partners (Fig. 2 *D*).

The biphasic binding of Ca^{2+} to CaM is well-documented in the literature by Bayley et al. (24) and others (25). This has been shown to occur due to the very rapid dissociation of Ca^{2+} from the N-ter EF-hand pair compared to its dissociation from the C-ter EF-hand pair, although some evidence suggests cooperative binding of Ca^{2+} to CaM (25). Black et al. have shown that a number of sequential kinetic models can predict binding response (26). Based on their results, Ca^{2+} binding to CaM was modeled using a four-step process, with two fast and two slow steps. In our model, we assumed that the fast steps are much faster than the slow steps and that therefore CaM$(Ca^{2+})_2$ and CaM$(Ca^{2+})_4$ are the only stable CaM- Ca^{2+} forms. Both species were assumed to bind to eNOS.

Besides CaM, another key regulator for eNOS activation under shear stress is Hsp90. Hsp90 does not bind to eNOS under static conditions, but significant binding was detected just 15 min after initiation of shear stress (27). CaM-bound eNOS has been shown to significantly increase the efficiency of Hsp90 recruitment (28). Studies have also shown that formation of the eNOS-CaM-Hsp90 complex is required for Akt-mediated eNOS phosphorylation on serine 1177 (29). Once phosphorylated, eNOS is stable in the active state, with enhanced NO production efficiency, until the phosphate group is removed. A quantitative model is created based on this scheme. All rate constants were either derived from existing models or optimized based on experimental data (see Supporting Material).

Model integration

All individual models were built using CellDesigner 4.1 (http://www.CellDesigner.org), a visual design tool for cell models and molecular pathways. Each model was coded in SBML, an XML-based format that is widely used to encode biomolecular pathways. SBML (4) was selected due to its open standard, the available programming interface, the LibSBML library (31), and its wide usage in the molecular modeling community and model repositories (such as http://www.Biomodels.net (30)). All models were encoded using the MIRIAM (minimum information requested in annotation of biochemical models) guidelines (3), which provide a rigorous set of information that mathematical models should include so that they can be reused.

An attractive feature of the SBML standard, combined with MIRIAM, is the ability to include the resource description framework (RDF) statements. These enable the unique identification of biomolecular components across multiple models irrespective of an individual model's notation. This is achieved by labeling elements (i.e., species, reactions, etc.) in external resources (ontologies or databases) that provide a mechanism for identifying common species and reactions across models. For a generic SBML- and MIRIAM-compliant model, it is possible to associate RDF statements to species, to reactions, and to the model itself, providing a means for performing more advanced processing and model merging. For example, a digital object identifier number or PubMed article identification provides a unique

link to a published article with the model details, and the universal resource identifier links to elements in the Systems Biology Ontology (32) or Chemical Entities of Biological Interest ontology (33) provide extensive information on individual biochemical species used within the model.

Writing each SBML model to be MIRIAM-compliant requires additional effort, but the RDF annotations enable models to be parsed and merged by a suitable logical reasoner. For this work, we used the ontology reasoning engine for molecular pathways (OREMP) computational code (34), which can automatically identify duplicate species across models. Moreover, OREMP can detect potential redundant reactions or reaction series that are shared across models. Identification of overlapping reactions is critical, because a hidden synergistic action of two or more separate mathematical statements of the same reaction leads to erroneous simulation results. The use of both species and reaction annotations becomes very useful in this process, as they enable the automatic match of cross-model components, minimizing user input. Using an ontological approach, the properties of each model discovered by the OREMP software can be appended to the description of the submodels, thus archiving these steps for future use.

The duplicate species and reactions between submodels provide the relevant information for model integration. They act as bindings that provide the map between individual model species and reactions within a single model and their interactions in the entire merged model. As newer models become available, they can also be integrated, either augmenting the current model or replacing redundant paths. This process differs significantly from the monolithic process, where each individual model is incorporated into a single model, requiring significantly more user effort.

Solving the model pathway

The partitioned models and their bindings provide the necessary information to simulate the global behavior of all interacting models. Models are aligned using CytoSolve and OREMP in combination, as outlined above, providing the detected duplicates as an editable list to the user. Once the bindings between models have been constructed, the user may then set up the necessary initial conditions, measured experimentally or estimated from computer optimization, for simulating the molecular pathway. Simulation is handled using libSBML to parse the original SBML models and SOSLib with SUNDIALS (35) to compute the evolution of submodels through time. CytoSolve solves the joint model not as a monolithic model but as a separated system of models. The merging of concentrations of individual model species is handled via a mass-balance controller, which ensures both that aligned bound species maintain the same concentration throughout the simulation and that the time steps taken are small enough to guarantee convergence of the separable solution to the true (monolithic) solution (see Ayyadurai and Dewey (5) and Nordsletten et al. (36) for further details).

RESULTS

A simulation of the integrated shear-stress-induced NO production model

When endothelial cells are exposed to shear stress, one of the first events is influx of calcium from extracellular space and intracellular storage. Fig. 3 *A* illustrates the concentration profile of intracellular calcium governed by the calcium influx model. The calcium level increases within the first 3 min after onset of shear stress; this transient response lasts for 10 min and quickly goes back to the resting-state level.

Another early event observed after onset of shear stress is activation of PI3K. The concentration profile (Fig. 3 *B*) of PI3K is simulated based on a time-dependent function generated from experimental data. Activation of PI3K is short and transient, but accumulation of PIP3 results in downstream Akt phosphorylation (Fig. 4 *A*). This result is consistent with experimental observations, where fully active AKT reaches the peak level within 30 min after onset of shear stress and gradually decays back to the initial state in hours (12,37).

A third early event after initiation of shear stress is activation of the focal adhesion complex, including

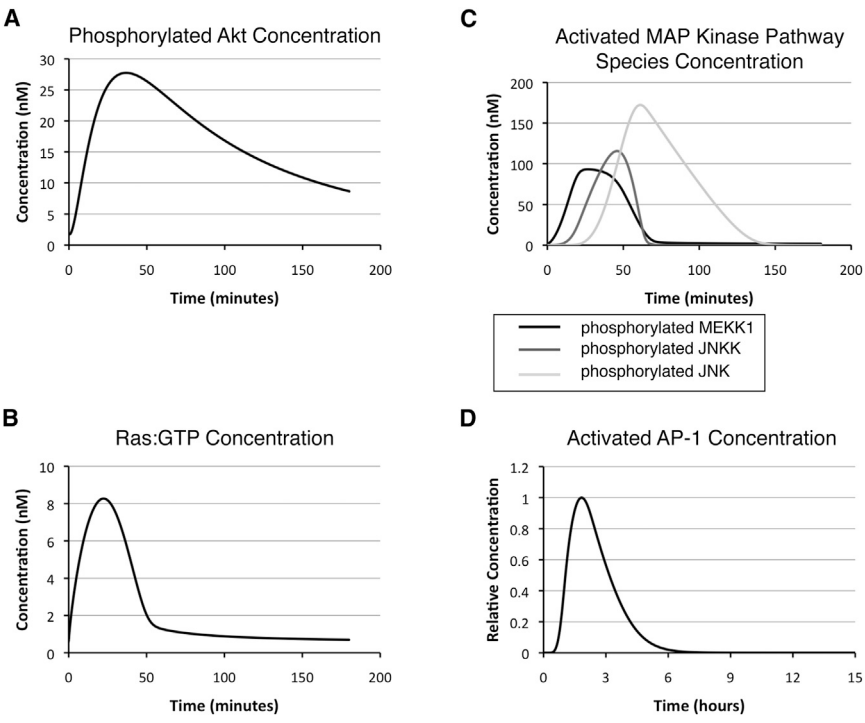

FIGURE 4 Simulation profiles of intermediate species upon initiation of shear stress. (*A*) Phosphorylated Akt (pp-Akt). (*B*) Ras/GTP. (*C*) Activated MAP kinase pathway species (p-MEKK1, pp-JNKK, and pp-JNK). (*D*) Activated AP-1.

phosphorylation of both focal adhesion kinase (FAK) and Src kinase (Fig. 3 *C*). Phosphorylation of the two proteins leads to downstream activation of Ras (Fig. 4 *B*) and the MAP kinase pathway proteins (Fig. 4 *C*) and subsequent AP-1 formation and nuclear translocation (Fig. 4 *D*). This process is transient, with a time span of a few hours, and is responsible for the fast-responding upregulation of eNOS mRNA and proteins after the cells experience a change in hemodynamic environment. Besides AP-1, the concentration profile for KLF2, another important transcription factor for eNOS, is shown in Fig. 3 *D*. KLF2 is responsible for long-term upregulation of eNOS mRNA and protein.

The above data describe the simulation results of individual pathways. These pathways interact with each other to control the dynamics of various eNOS species. Under the static (no-shear-stress) condition, eNOS primarily binds to Cav-1. After the onset of shear stress, calcium is transported to the cell and bound to CaM. Four calcium ions bind to each CaM to make the active form of CaM, which associates with eNOS to enhance its catalytic activity to produce NO (Fig. 5 *A*). In the meantime, the CaM-eNOS complex recruits Hsp90, which stabilizes the complex and facilitates Akt-mediated eNOS phosphorylation. The simulated concentration profile of eNOS phosphorylated on Ser-1177 (Fig. 5 *B*) is consistent with existing experimental observations (12) and depicts a biphasic pattern. In the first 10 min, when the phosphorylated Akt (enzyme) concentration is low but the CaM-eNOS-Hsp90 (substrate) concentration is high, there is rapid eNOS phosphorylation due to high substrate concentration. From 10 to 40 min, even though the substrate availability becomes low due to lower calcium concentration, the phosphorylated eNOS level stays high as a result of increasing phosphorylated Akt.

To maintain long-term NO production, a third mechanism employed by cells is increasing eNOS protein expression. Fig. 5, *C* and *D*, demonstrates the increase in eNOS mRNA and protein as catalyzed by the two transcription factors AP-1 and KLF2. The simulated expression of eNOS mRNA and protein under shear stress is shown with the experimental data from our lab and that of Li et al. (38), respectively. The concentration profile of eNOS mRNA also reveals a biphasic pattern as a result of early transcription by AP-1 and later transcription by KLF2. This biphasic effect is smoothed out after the eNOS translation process (Fig. 5 *D*).

Finally, the total NO production from eNOS is simulated under both static and shear-stress conditions. Fig. 6 shows the accumulated NO production over time from the integrated model. We used relative units for NO, since its experimentally observed concentration varies depending on the cell confluency and media volume of individual experimental setup. The simulated NO production profile resembles the experimental data measured by Florian et al. (39). Under static conditions, there is low NO production from background level of CaM-activated eNOS and phosphorylated eNOS. Under the shear-stress condition, calcium influx in the first few minutes leads to a quick burst

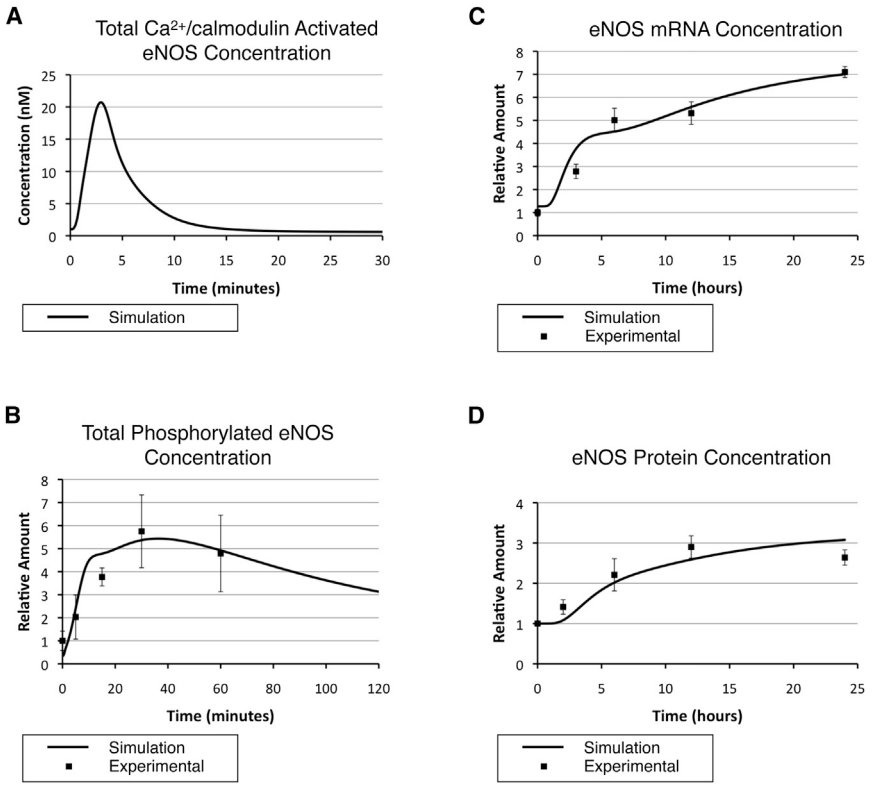

FIGURE 5 Simulation profiles of eNOS species. (*A*) Total Ca^{2+}/CaM-activated eNOS. (*B*) Total phosphorylated eNOS (Ser-1177). The simulated data are compared with experimental observations from Boo et al. (12). (*C*) eNOS mRNA. The simulated data are compared with our experimental observations. (*D*) Total eNOS protein. The simulated data are compared with experimental observations from Li et al. (38).

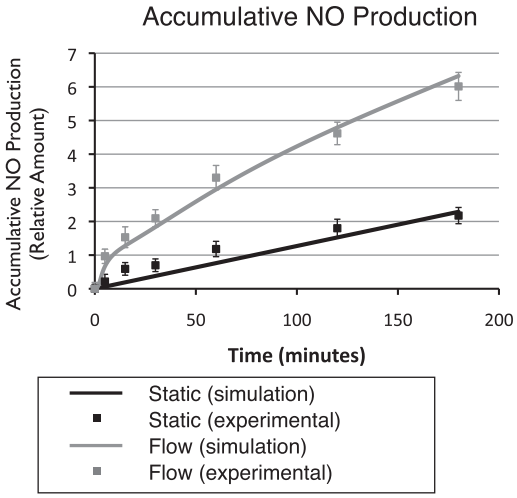

FIGURE 6 Comparison of the simulation results regarding cumulative NO production with experimental data (39) under static (no-shear-stress) and shear-stress conditions.

of NO production from CaM-activated eNOS. As calcium goes back to the basal level, phosphorylated eNOS kicks in to support NO production in the first few hours. The effect of eNOS expression does not come in until a few hours later (described in more detail in the next section).

The model integration approach provides insight into the system that could not be easily gathered experimentally

Having established a system model that allows us to simulate shear-stress-induced NO production comparable to that observed experimentally, we next explored several aspects of the system that can be simulated easily but are difficult to test experimentally. First, we analyzed the contribution of individual pathways to the overall NO production. The integrated modeling approach allows investigation of the relative importance of individual pathways instantaneously. Fig. 7 *A* demonstrates the cumulative NO production contributed by different eNOS species. The data show that almost all of the NO produced in the first 10 min comes from Ca^{2+}/CaM-activated eNOS, with later production of NO mostly contributed by phosphorylated eNOS. In contrast, the NO produced by the intermediate species, Ca^{2+}/CaM-activated phosphorylated eNOS, is not significant.

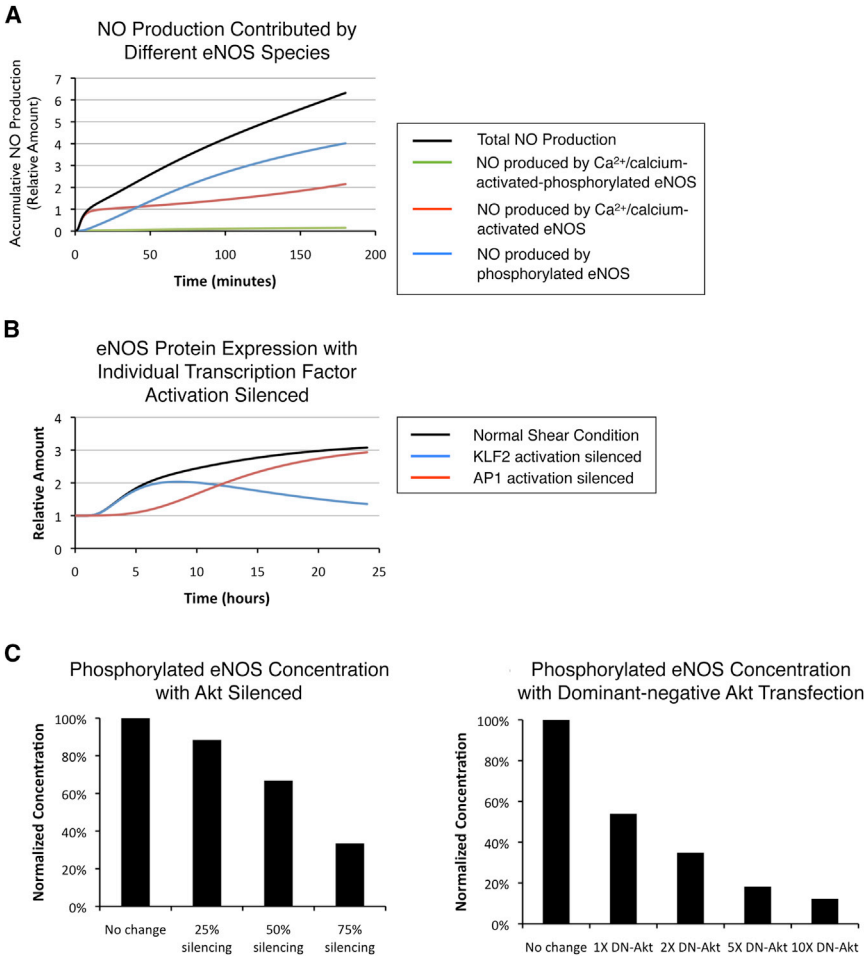

FIGURE 7 The integrated model allows us to easily assess the contribution of individual eNOS species or simulate the condition where one pathway is modified. (*A*) Contribution of NO production by different eNOS species. (*B*) eNOS protein expression with individual transcription-factor activation silenced. Concentrations of the specific transcription factor are fixed at the static level. (*C*) Normalized concentration of total phosphorylated eNOS with addition of Akt siRNA (*left*) or dominant-negative Akt (*right*) 1 h after onset of shear stress. In the Akt siRNA simulation, total Akt concentration was reduced based on the specific silencing efficiency. In the dominant-negative Akt (DN-Akt) simulation, DN-Akt follows the exact kinetics of wild-type Akt except that it loses its catalytic ability to phosphorylate eNOS. The amount of wild-type Akt remains constant, whereas the amount of DN-Akt is 1×, 2×, 5×, and 10× the amount of wild-type Akt.

Second, we simulate the small-interfering RNA (siRNA) gene-silencing approaches by selectively silencing shear-stress-induced activation of individual pathways. This process can be easily illustrated by removing or modifying species in the system, giving reasonable predictions while saving tremendous resources. In the NO system, we assess the effect of modifying individual pathways on overall NO production. To research how an individual transcription factor affects overall eNOS protein expression, AP-1 and KLF2 activation were blocked (Fig. 7 *B*). Blocking AP-1 activation yields a delayed response in eNOS expression under shear stress, whereas blocking KLF2 activation leads to no shear-stress-induced eNOS expression after 24 h.

Finally, we attempt to predict the effect of transfecting endothelial cells with Akt siRNA or dominant-negative Akt on eNOS phosphorylation (Fig. 7 *C*) under 1 h of shear stress. Our simulation data suggest that the relationship between silencing efficiency and the resulting decrease in eNOS phosphorylation is not linear. An Akt knockdown efficiency of 25% has little effect on eNOS phosphoryation, a 50% efficiency still retains >60% of phosphorylated eNOS; it is not until a 75% silencing efficiency is achieved that we observe <40% eNOS phosphorylation. A similar effect of decreasing eNOS phosphorylation can be achieved with an alternative approach. Fisslthaler et al. have demonstrated that transfecting the cells with dominant-negative Akt (DN-Akt) decreases shear-stress-induced eNOS phosphorylation (13). Here, we simulate the condition in which there are various amounts of DN-Akt (1×, 2×, 5×, and 10× relative to wild-type) in the system in addition to wild-type eNOS. DN-Akt competes with the wild-type Akt for the binding site on the plasma membrane and significantly reduces shear-stress-activated eNOS phosphorylation.

It is important to note that when a known pathway is knocked down, which, for a given pathway, would yield no shear-stress-induced NO production, the integrated model shows robustness to the knockdown of that specific pathway (e.g., Akt) but fails to take into account alternative ones (e.g., PKA, AMPK). This result emphasizes the importance of systems biology for achieving a quantitative understanding of macroscopic cellular response processes, as well as the power of such analyses for more comprehensive pathway assessment. However, this result also highlights a major limitation of the approach, which is the absolute dependence of previously reported and characterized data on defined signaling pathways that can be incorporated into a model (e.g., Akt versus PKA versus AMPK).

DISCUSSION

The power of automatic model integration

Quantitative modeling of molecular pathways provides a powerful tool for simulating and predicting function. With more and more comprehensive experimental data, it is rapidly becoming possible to construct more complete models of molecular pathways. A major bottleneck in this process, however, is the current model paradigm where models are manually integrated into a single complex model, obscuring the link to previously published pathways. In this article, we introduced an alternative model-binding approach in which individual models are written and retained as is standard in MIRIAM-compliant SBML format. The alterations, duplicate species, and duplicate reactions are then detailed within the model bindings, providing clarity on how past models are incorporated into the current model. The tools for this merger process, as well as the simulation of merged models, have been made available, as part of our continued work, by CytoSolve.

In this study, we considered four primary pathways that govern the activation and transcription/translation of eNOS, the NO catalyst. All these paths have been shown to work in tandem to govern the transient NO response of cells to shear stress. Indeed, we show that the NO response consists of three primary phases that act on varying timescales. The transient response is thus governed by the ensemble of molecular pathways and cannot be accurately modeled by considering any component individually. In addition to illustrating the need for model integration, the introduced pathways demonstrate the power of the model-binding approach. As the system is composed of individual models, additional pathway models based on new experimental data can be quickly incorporated into the system without rewriting the existing model. It also allows us to easily investigate the relative contribution of each pathway and conduct in silico experiments as demonstrated in Fig. 7.

Utilizing MIRIAM standards and references to web-accessible ontologies, this study also introduced an approach for automating model integration. This strategy is the opposite of the monolithic approach in which many models are manually assembled to compose a single new model that is more difficult to further edit, generally resulting in valued work with limited reusability. In contrast to this approach, the partitioned approach introduced in this work provides an additive model-creation paradigm, where previous knowledge, data, and effort can easily be managed, curated, and used by the wider scientific community. This is accomplished by the model-binding approach, where individual models retain their original identity. The bindings between individual models provide the necessary interface for both defining how an original model is used and altered, preserving the original model and its lineage and making the modeling process more straightforward. In addition, the integration of models via the partitioned approach makes much more straightforward the process of updating the model while at the same time preserving the extant bindings and models.

Limitations in shear-stress-induced NO pathway modeling

In this article, we collect the relevant pathways, species, and reactions to reflect the state-of-the-art understanding of NO production. Although the NO system provides a quantitative link between shear stress and NO production through activation and transcription pathways that match well with published experimental data, further work is required to improve and enhance the model. Due to limitations in available data, some model components were based on experiments using different endothelial cell types, as well as different experimental conditions (variations in culture conditions and mechanisms for applying shear). Although these issues are not unique to this model, but are common to a number of cellular models, they warrant further experimental investigation and validation. These weaknesses can be annotated in the model and made transparent for future improvement. Despite these limitations, the model does demonstrate the general dynamics of multiple pathways acting in concert to upregulate NO production.

To further improve the integrated NO model, incorporation of other mechanotransduction pathways is necessary. For example, the endothelial glycocalyx has been shown to be an important mechanosensor for shear-stress-induced NO production. Treating the endothelial surface with heparanase to remove heparan sulfate, one major glycosaminoglycan of the glycocalyx layer, significantly reduces NO production resulting from shear stress (39,40). The specific signaling pathways that trigger the models used here are still not known. Moreover, we have used a simple heuristic model based on experimental data to represent the upregulation of KLF2 by shear stress. KLF2, a key regulator for eNOS expression, is also a shear-responding transcription factor leading to antiinflammatory and antithrombotic phenotypes (41). KLF2 expression is known to follow the MEK5-ERK5-MEF2 pathway, but the mechanosensors that lead to the activation of this pathway are still unclear (23). These additions are currently limited by incomplete knowledge of pathway mechanisms and lack of critical kinetic data. However, the current integrated model creates a platform to identify deficiencies in our current understanding, provide more suitable parameters, and embed additional pathways or information in an additive way. This process acts as a communal way of documenting what is understood about cellular mechanisms of NO production in endothelial cells.

Future model integration tools and development

This article outlines the use of CytoSolve in facilitating model integration. Although this tool automates the model integration process with minimal input from the user, further development could dramatically improve the effectiveness of the integration process, store relevant changes at various stages in development, and provide tools for incorporating input from the wider scientific community.

One of the major aims of this work was to demonstrate that the combination of separate biological models to generate a new, larger predictive model is difficult but becomes tractable with the right tools. Because a model that exists completely independently of other models is of limited use to the research community, it behooves the community to define processes by which existing and new models can be augmented, combined, and increased in complexity so that existing work is properly assimilated.

It is also important to recognize that different models have different aims and often operate at different timescales, spatial scales, and initial conditions; most of the models have species exchanges on the order of μM/min or nM/min, but this is not universally suitable for every objective. Because SBML makes it possible to define arbitrary units by composing IS units, it is among CytoSolve's goals to resolve and normalize differing units in a transparent manner. A new algorithm will extend the current mass-balance, introducing a unit-conversion routine that will be called at run time, keeping the merged solution independent of any individual model's representation.

Another future addition will be the extension of the actual cross-model information-sharing process to show users other reactions that may be of interest to them. This will provide an autocompletion for models to include reactions seen in other models. The goal of this functionality is to accelerate the information-sharing and model-composition process even more: building models on top of others, reducing unnecessary duplicates, and informing researchers of known existing pathways that may be relevant to their study.

CONCLUSION

In this study, we simulated the process of shear-stress-induced NO production in endothelial cells by combining a number of existing published pathway models to describe and predict the complex interactions that occur between them at multiple timescales. The program we used, CytoSolve, is specifically designed to facilitate the federation of individual biological pathways in a manner that allows them to run as a combined monolithic model without losing their individuality and the metadata attached to them. The integrated model reflects the state-of-the-art understanding of the NO system, and the simulation data are able to describe experimental observations resulting from complex interactions between multiple pathways. The system-level simulation approach can also provide researchers with useful insights into the system that have traditionally only been achieved with challenging and time-consuming experiments. It is important to note that this approach to biological pathway integration is not only helpful for our understanding of biological system, but it also provides a

platform to aggregate information in an additive way, which eventually could allow us to predict biology.

SUPPORTING MATERIAL

Four models and their lists of parameters, as well as Supporting Methods, and references (42–47) are available at http://www.biophysj.org/biophysj/supplemental/S0006-3495(13)00391-3.

We thank Akila Surendran, Manuel Legrand, Jacqueline Wentz, and John Yazbek for help creating the preliminary models.

This study was funded by a grant from the National Institutes of Health (R01HL090856). We also acknowledge support from the Singapore-MIT Computational and Systems Biology Program.

REFERENCES

1. Sessa, W. C. 2004. eNOS at a glance. *J. Cell Sci.* 117:2427–2429.
2. Niederer, S. A., M. Fink, …, N. P. Smith. 2009. A meta-analysis of cardiac electrophysiology computational models. *Exp. Physiol.* 94: 486–495.
3. Le Novère, N., A. Finney, …, B. L. Wanner. 2005. Minimum information requested in the annotation of biochemical models (MIRIAM). *Nat. Biotechnol.* 23:1509–1515.
4. Hucka, M., A. Finney, …, J. Wang; SBML Forum. 2003. The systems biology markup language (SBML): a medium for representation and exchange of biochemical network models. *Bioinformatics.* 19:524–531.
5. Ayyadurai, V. A., and C. F. Dewey. 2011. CytoSolve: a scalable computational method for dynamic integration of multiple molecular pathway models. *Cell Mol. Bioeng.* 4:28–45.
6. Davies, P. F. 1995. Flow-mediated endothelial mechanotransduction. *Physiol. Rev.* 75:519–560.
7. Chachisvilis, M., Y. L. Zhang, and J. A. Frangos. 2006. G protein-coupled receptors sense fluid shear stress in endothelial cells. *Proc. Natl. Acad. Sci. USA.* 103:15463–15468.
8. Wiesner, T. F., B. C. Berk, and R. M. Nerem. 1997. A mathematical model of the cytosolic-free calcium response in endothelial cells to fluid shear stress. *Proc. Natl. Acad. Sci. USA.* 94:3726–3731.
9. Wiesner, T. F., B. C. Berk, and R. M. Nerem. 1996. A mathematical model of cytosolic calcium dynamics in human umbilical vein endothelial cells. *Am. J. Physiol.* 270:C1556–C1569.
10. Dimmeler, S., I. Fleming, …, A. M. Zeiher. 1999. Activation of nitric oxide synthase in endothelial cells by Akt-dependent phosphorylation. *Nature.* 399:601–605.
11. Balligand, J.-L., O. Feron, and C. Dessy. 2009. eNOS activation by physical forces: from short-term regulation of contraction to chronic remodeling of cardiovascular tissues. *Physiol. Rev.* 89:481–534.
12. Boo, Y. C., G. Sorescu, …, H. Jo. 2002. Shear stress stimulates phosphorylation of endothelial nitric-oxide synthase at Ser1179 by Akt-independent mechanisms: role of protein kinase A. *J. Biol. Chem.* 277:3388–3396.
13. Fisslthaler, B., S. Dimmeler, …, I. Fleming. 2000. Phosphorylation and activation of the endothelial nitric oxide synthase by fluid shear stress. *Acta Physiol. Scand.* 168:81–88.
14. Koh, G., H. F. C. Teong, …, P. S. Thiagarajan. 2006. A decompositional approach to parameter estimation in pathway modeling: a case study of the Akt and MAPK pathways and their crosstalk. *Bioinformatics.* 22:e271–e280.
15. Go, Y. M., H. Park, …, H. Jo. 1998. Phosphatidylinositol 3-kinase γ mediates shear stress-dependent activation of JNK in endothelial cells. *Am. J. Physiol.* 275:H1898–H1904.
16. Won, D., S. N. Zhu, …, M. I. Cybulsky. 2007. Relative reduction of endothelial nitric-oxide synthase expression and transcription in atherosclerosis-prone regions of the mouse aorta and in an in vitro model of disturbed flow. *Am. J. Pathol.* 171:1691–1704.
17. Chen, K. D., Y. S. Li, …, J. Y. Shyy. 1999. Mechanotransduction in response to shear stress. Roles of receptor tyrosine kinases, integrins, and Shc. *J. Biol. Chem.* 274:18393–18400.
18. Hatakeyama, M., S. Kimura, …, A. Konagaya. 2003. A computational model on the modulation of mitogen-activated protein kinase (MAPK) and Akt pathways in heregulin-induced ErbB signalling. *Biochem. J.* 373:451–463.
19. Li, S., M. Kim, …, J. Y. Shyy. 1997. Fluid shear stress activation of focal adhesion kinase. Linking to mitogen-activated protein kinases. *J. Biol. Chem.* 272:30455–30462.
20. Jalali, S., Y. S. Li, …, J. Y. Shyy. 1998. Shear stress activates p60src-Ras-MAPK signaling pathways in vascular endothelial cells. *Arterioscler. Thromb. Vasc. Biol.* 18:227–234.
21. Kholodenko, B. N. 2000. Negative feedback and ultrasensitivity can bring about oscillations in the mitogen-activated protein kinase cascades. *Eur. J. Biochem.* 267:1583–1588.
22. Young, A., W. Wu, …, G. García-Cardeña. 2009. Flow activation of AMP-activated protein kinase in vascular endothelium leads to Krüppel-like factor 2 expression. *Arterioscler. Thromb. Vasc. Biol.* 29:1902–1908.
23. Parmar, K. M., H. B. Larman, …, G. García-Cardeña. 2006. Integration of flow-dependent endothelial phenotypes by Kruppel-like factor 2. *J. Clin. Invest.* 116:49–58.
24. Bayley, P., P. Ahlström, …, S. Forsen. 1984. The kinetics of calcium binding to calmodulin: Quin 2 and ANS stopped-flow fluorescence studies. *Biochem. Biophys. Res. Commun.* 120:185–191.
25. Linse, S., A. Helmersson, and S. Forsén. 1991. Calcium binding to calmodulin and its globular domains. *J. Biol. Chem.* 266:8050–8054.
26. Black, D. J., J. E. Selfridge, and A. Persechini. 2007. The kinetics of Ca^{2+}-dependent switching in a calmodulin-IQ domain complex. *Biochemistry.* 46:13415–13424.
27. García-Cardeña, G., R. Fan, …, W. C. Sessa. 1998. Dynamic activation of endothelial nitric oxide synthase by Hsp90. *Nature.* 392:821–824.
28. Gratton, J. P., J. Fontana, …, W. C. Sessa. 2000. Reconstitution of an endothelial nitric-oxide synthase (eNOS), hsp90, and caveolin-1 complex in vitro. Evidence that hsp90 facilitates calmodulin stimulated displacement of eNOS from caveolin-1. *J. Biol. Chem.* 275:22268–22272.
29. Dudzinski, D. M., and T. Michel. 2007. Life history of eNOS: partners and pathways. *Cardiovasc. Res.* 75:247–260.
30. Le Novère, N., B. Bornstein, …, M. Hucka. 2006. BioModels Database: a free, centralized database of curated, published, quantitative kinetic models of biochemical and cellular systems. *Nucleic Acids Res.* 34(Database issue):D689–D691.
31. Bornstein, B. J., S. M. Keating, …, M. Hucka. 2008. LibSBML: an API library for SBML. *Bioinformatics.* 24:880–881.
32. Courtot, M., N. Juty, …, N. Le Novère. 2011. Controlled vocabularies and semantics in systems biology. *Mol. Syst. Biol.* 7:543.
33. Degtyarenko, K., P. de Matos, …, M. Ashburner. 2008. ChEBI: a database and ontology for chemical entities of biological interest. *Nucleic Acids Res.* 36(Database issue):D344–D350.
34. Umeton, R., G. Nicosia, and C. F. Dewey, Jr. 2012. OREMPdb: a semantic dictionary of computational pathway models. *BMC Bioinformatics.* 13(*Suppl 4*):S6.
35. Machné, R., A. Finney, …, C. Flamm. 2006. The SBML ODE Solver Library: a native API for symbolic and fast numerical analysis of reaction networks. *Bioinformatics.* 22:1406–1407.
36. Nordsletten, D. A., B. Yankama, …, C. F. Dewey, Jr. 2011. Multiscale mathematical modeling to support drug development. *IEEE Trans. Biomed. Eng.* 58:3508–3512.

37. Dimmeler, S., B. Assmus, …, A. M. Zeiher. 1998. Fluid shear stress stimulates phosphorylation of Akt in human endothelial cells: involvement in suppression of apoptosis. *Circ. Res.* 83:334–341.

38. Li, Y., J. Zheng, …, R. R. Magness. 2005. Effects of pulsatile shear stress on signaling mechanisms controlling nitric oxide production, endothelial nitric oxide synthase phosphorylation, and expression in ovine fetoplacental artery endothelial cells. *Endothelium.* 12:21–39.

39. Florian, J. A., J. R. Kosky, …, J. M. Tarbell. 2003. Heparan sulfate proteoglycan is a mechanosensor on endothelial cells. *Circ. Res.* 93:e136–e142.

40. Pahakis, M. Y., J. R. Kosky, …, J. M. Tarbell. 2007. The role of endothelial glycocalyx components in mechanotransduction of fluid shear stress. *Biochem. Biophys. Res. Commun.* 355:228–233.

41. Dekker, R. J., S. van Soest, …, A. J. Horrevoets. 2002. Prolonged fluid shear stress induces a distinct set of endothelial cell genes, most specifically lung Krüppel-like factor (KLF2). *Blood.* 100:1689–1698.

42. Yamada, S., S. Shiono, …, A. Yoshimura. 2003. Control mechanism of JAK/STAT signal transduction pathway. *FEBS Lett.* 534:190–196.

43. Yee, K. L., V. M. Weaver, and D. A. Hammer. 2008. Integrin-mediated signalling through the MAP-kinase pathway. *IET Syst. Biol.* 2:8–15.

44. Weber, M., C. H. Hagedorn, …, C. D. Searles. 2005. Laminar shear stress and 3′ polyadenylation of eNOS mRNA. *Circ. Res.* 96:1161–1168.

45. Kuchan, M. J., and J. A. Frangos. 1994. Role of calcium and calmodulin in flow-induced nitric oxide production in endothelial cells. *Am. J. Physiol.* 266:C628–C636.

46. Liu, J., G. García-Cardeña, and W. C. Sessa. 1995. Biosynthesis and palmitoylation of endothelial nitric oxide synthase: mutagenesis of palmitoylation sites, cysteines-15 and/or -26, argues against depalmitoylation-induced translocation of the enzyme. *Biochemistry.* 34:12333–12340.

47. Schwarz, G., G. Droogmans, and B. Nilius. 1992. Shear stress induced membrane currents and calcium transients in human vascular endothelial cells. *Pflugers Arch.* 421:394–396.

48. Wedgwood, S., C. J. Mitchell, …, S. M. Black. 2003. Developmental differences in the shear stress-induced expression of endothelial NO synthase: changing role of AP-1. *Am. J. Physiol. Lung Cell. Mol. Physiol.* 284:L650–L662.

49. Wang, Y., J. Chang, …, S. Chien. 2004. Shear stress and VEGF activate IKK via the Flk-1/Cbl/Akt signaling pathway. *Am. J. Physiol. Heart Circ. Physiol.* 286:H685–H692.

50. Davis, M. E., I. M. Grumbach, …, D. G. Harrison. 2004. Shear stress regulates endothelial nitric-oxide synthase promoter activity through nuclear factor κB binding. *J. Biol. Chem.* 279:163–168.

51. García-Cardeña, G., R. Fan, …, W. C. Sessa. 1996. Endothelial nitric oxide synthase is regulated by tyrosine phosphorylation and interacts with caveolin-1. *J. Biol. Chem.* 271:27237–27240.

52. Förstermann, U., J. S. Pollock, …, F. Murad. 1991. Calmodulin-dependent endothelium-derived relaxing factor/nitric oxide synthase activity is present in the particulate and cytosolic fractions of bovine aortic endothelial cells. *Proc. Natl. Acad. Sci. USA.* 88:1788–1792.

53. Fontana, J., D. Fulton, …, W. C. Sessa. 2002. Domain mapping studies reveal that the M domain of hsp90 serves as a molecular scaffold to regulate Akt-dependent phosphorylation of endothelial nitric oxide synthase and NO release. *Circ. Res.* 90:866–873.

In Silico Modeling of Shear-Stress-Induced Nitric Oxide Production in Endothelial Cells through Systems Biology

Andrew Koo,[†||] David Nordsletten,[¶] Renato Umeton,[‡] Beracah Yankama,[§] Shiva Ayyadurai,[†] Guillermo García-Cardeña,[||] and C. Forbes Dewey, Jr.[†‡]*

[†]Department of Biological Engineering, [‡]Department of Mechanical Engineering, and [§]Laboratory for Information and Decision Systems, Massachusetts Institute of Technology, Cambridge, Massachusetts; [¶]Department of Biomedical Engineering, King's College London, London, United Kingdom; and [||]Laboratory for Systems Biology, Center for Excellence in Vascular Biology, Department of Pathology, Brigham and Women's Hospital and Harvard Medical School, Boston, Massachusetts

Koo et al.

Modeling Shear-Induced NO Production

*Correspondence: cfdewey@mit.edu

SUPPORTING MATERIAL

Model Reactions and Parameters

Model 1: Shear-stress-induced calcium influx

Model Diagram (Figure legends at the end of appendix):

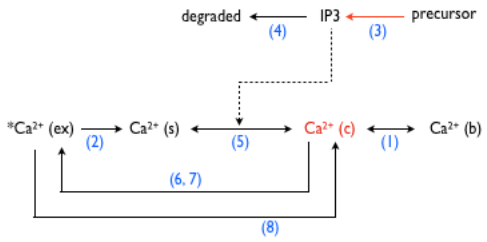

List of species:

Species	Name	Initial Amount	Ref.
Ca^{2+} (b)	Calcium complexed to intracellular binding proteins	3870 nM	(1)
Ca^{2+} (ex)	Extracellular calcium	$1.5 * 10^6$ nM	(1)
Ca^{2+} (s)	Calcium in intracellular storage	$2.83 * 10^6$ nM	(1)
Ca^{2+} (c)	Cytosolic calcium	117.2 nM	Steady state value for the integrated model under "no flow" condition
IP3	Inositol 1,4,5-triphosphate	0 nM	(1)

List of reactions:

#	Description	Rate equation	Ref.
1	$[Ca^{2+}$ (b)$] \leftrightarrow [Ca^{2+}$ (c)$]$	$k_7[Ca^{2+}(b)] - k_6[Ca^{2+}(c)] \cdot (B_T - [Ca^{2+}(b)])$	(1)
2	$[Ca^{2+}$ (ex)$] \rightarrow [Ca^{2+}$ (s)$]$	$k_{CCE} \cdot (\frac{fracK \cdot Ca_0^{2+}}{K3 + Ca_0^{2+}} - [Ca^{2+}(s)]) \cdot ([Ca^{2+}(ex)] - [Ca^{2+}(s)])$	(1)
3	$\phi \rightarrow$ [IP3]	$k_1 \cdot (R_T - \frac{R_T}{2} \cdot (e^{-t/\tau_I} + e^{-t/\tau_{II}}) + \left(\frac{\tau_I + \tau_{II}}{\tau_I - \tau_{II}}\right) \cdot (e^{-t/\tau_I} - e^{-t/\tau_{II}})) \cdot \left(\frac{[Ca^{2+}(c)]}{K_1 + [Ca^{2+}(c)]}\right)$	(1)
4	[IP3] $\rightarrow \phi$	$k_2[IP3]$	(1)
5	$[Ca^{2+}$ (s)$] \leftrightarrow [Ca^{2+}$ (c)$]$	$k_3 \frac{k_{CICR}[Ca^{2+}(c)]}{K_{CICR} + [Ca^{2+}(c)]} \cdot \left(\frac{[IP3]}{K_2 + [IP3]}\right)^3 \cdot [Ca^{2+}(s)] - k_4\left(\frac{[Ca^{2+}(c)]}{K_3 + [Ca^{2+}(c)]}\right)^2 + k_5\left([Ca^{2+}(s)]\right)^2$	(1)
6	$[Ca^{2+}$ (c)$] \rightarrow [Ca^{2+}$ (ex)$]$	$\dot{V}_{ex} \frac{[Ca^{2+}(c)]}{K_5 + [Ca^{2+}(c)]}$	(1)
7	$[Ca^{2+}$ (c)$] \rightarrow [Ca^{2+}$ (ex)$]$	$\dot{V}_p \frac{\left([Ca^{2+}(c)]\right)^2}{K_4^2 + \left([Ca^{2+}(c)]\right)^2} + \dot{V}_{hi} \frac{\left([Ca^{2+}(c)]\right)^4}{K_{hi}^4 + \left([Ca^{2+}(c)]\right)^4}$	(1)
8	$[Ca^{2+}$ (ex)$] \rightarrow [Ca^{2+}$ (c)$]$	$\dot{Q}_{shear}$	(2)

List of parameters:

	Units	Ref.	Ref. value	Model value
R_T	# / cell	(1)	$4.4 * 10^4$	$4.4 * 10^4$
k_1	nM • s^{-1}	(1)	$1.2 * 10^{-3}$	$6.0 * 10^{-4}$
k_2	s^{-1}	(1)	2	1
k_3	s^{-1}	(1)	6.64	3.32
k_4	nM • s^{-1}	(1)	5000	2500
k_5	nM^{-1} • s^{-1}	(1)	$1.0 * 10^{-10}$	$5.0 * 10^{-11}$
k_6	nM^{-1} • s^{-1}	(1)	0.1	0.05
k_7	s^{-1}	(1)	300	150
K_1	nM	(1)	0	0
K_2	nM	(1)	200	200
K_3	nM	(1)	150	150
K_4	nM	(1)	80	80
K_5	nM	(1)	321	321
K_{hi}	nM	(1)	380	380
k_{CICR}	dimensionless	(1)	1	1
K_{CICR}	nM	(1)	0	0
k_{CCE}	nM^{-1} • s^{-1}	(1)	0	0
B_T	nM	(1)	$1.2 * 10^5$	$1.2 * 10^5$
Ca_0^{2+}	nM	(1)	100	100
$\dot{Q}_{shear}$	nM^{-1} • s^{-1}	(2), based on 10 dynes/cm^2	6000	3000
$\dot{V}_p$	nM^{-1} • s^{-1}	(1)	1630	815
$\dot{V}_{ex}$	nM^{-1} • s^{-1}	(1)	18330	9165
$\dot{V}_{hi}$	nM^{-1} • s^{-1}	(1)	4760	2380

τ_I	s	(1)	33	66
τ_{II}	s	(1)	0.005	0.01
fracK	dimensionless	(1)	$7.1 * 10^6$	$7.1 * 10^6$

References for model 1:
(1, 2)

Model 2: Shear-stress-induced AKT phosphorylation

Model Diagram:

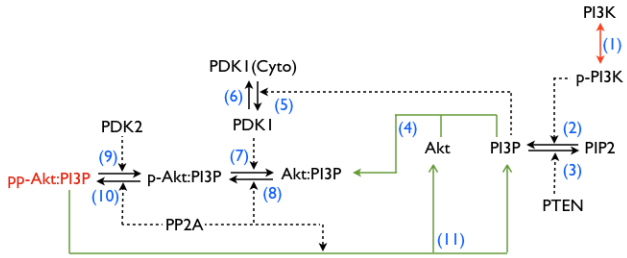

List of species:

Species	Name	*Initial Amount	Ref.
PI3K	PI 3-kinases	99.97 nM	Total PI3K concentration 100 nM (3)
p-PI3K	Phosphorylated PI 3-kinases	0.03 nM	---
PIP2	Phosphatidylinositol-4,5-biphosphate	6967.27 nM	Total PIP2 concentration 7000 nM (3)
PI3P	Phosphatidylinositol-3,4,5-triphosphate	0.35 nM	---
PTEN	Phosphatase and tensin homolog	0.1 nM	Constant (3)
Akt	Akt, or Protein Kinase B	167.62 nM	Total Akt concentration 200 nM (3)
Akt: PI3P	Membrane bound Akt	29.2 nM	---
p-Akt:PI3P	Monophosphorylated Akt	1.46 nM	---
pp-Akt:PI3P	Biphosphorylated Akt	1.72 nM	---
PDK1 (cyto)	Cytosolic phosphoinositide-dependent kinase-1	999.75 nM	Total PDK1 concentration 1000 nM (3)
PDK1	Phosphoinositide-dependent kinase-1	0.25 nM	---
PDK2	Phosphoinositide-dependent kinase-2	3 nM	Constant (3)
PP2A	Protein phosphatase 2	150 nM	Constant (3)

*** Initial amounts were obtained by simulating the model under "no flow" condition, with the reference value as initial concentrations, for a sufficient amount of time to reach steady state.**

List of reactions:

#	Description	Rate equation	Ref.
*1	[PI3K] ↔ [p-PI3K]	$\exp(1-\left(\frac{t}{15}\right)^{1.8})\cdot 0.907\cdot t^{0.8}\cdot(1-\left(\frac{t}{15}\right)^{1.8})$	(4)
2	[PIP2] → [PI3P]	$k_2\frac{[p-PI3K][PIP2]}{K_{m2}+[PIP2]}$	(3)
3	[PI3P] → [PIP2]	$k_3\frac{[PTEN][PI3P]}{K_{m3}+[PI3P]}$	(3)
4	[Akt] + [PI3P] ↔ [Akt:PI3P]	$k_4[PI3P][Akt]-k_{r4}[Akt:PI3P]$	(3)
5	[PDK1 (cyto)] → [PDK1]	$k_5[PI3P][PDK1]$	(3)
6	[PDK1] → [PDK1 (cyto)]	$k_6[PDK1]$	(3)
7	[p-Akt:PI3P] → [Akt:PI3P]	$k_7\frac{[PP2A][p-Akt:PI3P]}{K_{m7}+[p-Akt:PI3P]}$	(3)

8	[Akt:PI3P] → [p-Akt:PI3P]	$k_8 \frac{[PDK1][Akt:PI3P]}{K_{m8}+[Akt:PI3P]}$	(3)
9	[pp-Akt:PI3P] → [p-Akt:PI3P]	$k_9 \frac{[PP2A][pp-Akt:PI3P]}{K_{m9}+[pp-Akt:PI3P]}$	(3)
10	[p-Akt:PI3P] → [pp-Akt:PI3P]	$k_{10} \frac{[PDK2][Akt:PI3P]}{K_{m10}+[Akt:PI3P]}$	(3)
11	[pp-Akt:PI3P] → [Akt] + [PI3P]	$k_{11} \frac{[PP2A][pp-Akt:PI3P]}{K_{m11}+[pp-Akt:PI3P]}$	(3)

*** Time-dependent function describing PI3K activation was generated from the experimental data in [4]. The shear stress waveform used in this paper is a laminar flow of 5 dynes/cm^2.**

List of parameters:

	Units	**Ref.**	**Ref. value**	**Model value**
k_2	s^{-1}	(3)	0.05	0.2
K_{m2}	nM	(3)	6170	6170
k_3	s^{-1}	(3)	5.5	7.5
K_{m3}	nM	(3)	80.9	80.9
k_4	$nM^{-1} \bullet s^{-1}$	(3)	0.045	0.045
k_{r4}	s^{-1}	(3)	0.089	0.089
k_5	$nM^{-1} \bullet s^{-1}$	(3)	0.0007	0.0007
k_6	s^{-1}	(3)	0.98	0.98
k_7	s^{-1}	(3)	0.037	0.037
K_{m7}	nM	(3)	8800	8800
k_8	s^{-1}	(3)	20	20
K_{m8}	nM	(3)	80000	80000
k_9	s^{-1}	(3)	0.04	0.04
K_{m9}	nM	(3)	48000	48000
k_{10}	s^{-1}	(3)	20	20
K_{m10}	nM	(3)	80000	80000
k_{11}	s^{-1}	(3)	0.163	0.163
K_{m11}	nM	(3)	48000	48000

References for model 2:

(3, 4)

Model 3: Shear-stress-induced eNOS expression

Model Diagram:

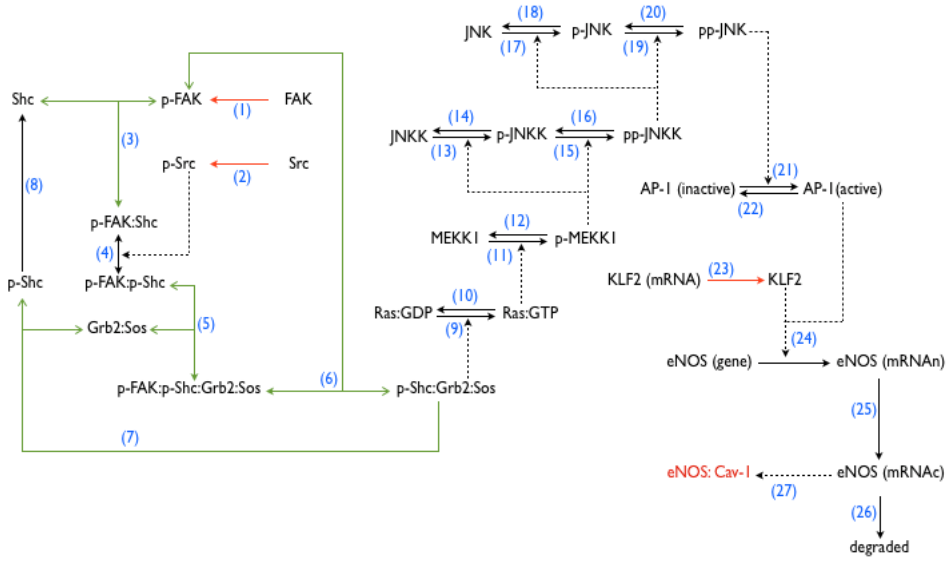

List of species:

Species	**Name**	***Initial Amount**	**Ref.**
FAK	Focal adhesion kinase	57 nM	Total FAK concentration 80 nM (7)
p-FAK	Phosphorylated FAK	0.605 nM	---
Src	Src kinase	72 nM	Total Src concentration 90 nM (7)
p-Src	Phosphorylated Src	18 nM	---
Shc	Shc adaptor protein	819.25 nM	Total Shc concentration 1000 nM (8)
p-FAK:Shc	Protein complex	0.857 nM	---
p-FAK:p-Shc	Protein complex	15.962 nM	---
Grb2:Sos	Grb2:Sos adaptor protein	3.23 nM	Total Grb2:Sos concentration 10 nM (8)
p-FAK:p-Shc:Grb2:Sos	Protein complex	5.577 nM	---
p-Shc:Grb2:Sos	Protein complex	1.193 nM	---
p-Shc	Phosphorylated Shc	157.162 nM	---
Ras:GDP	Ras protein (GDP state)	119.384 nM	Total Ras concentration 120 nM (8)
Ras:GTP	Ras protein (GTP state)	0.616 nM	---
MEKK1	MEKK1 kinase	98.514 nM	Total MEKK1 concentration 100 nM (10)
p-MEKK1	Phosphorylated MEKK1	1.486 nM	---
JNKK	JNK-activated kinase	299.706 nM	Total JNKK concentration 300 nM (10)
p-JNKK	Monophosphorylated JNKK	0.288 nM	---
pp-JNKK	Biphosphorylated JNKK	0.006 nM	---
JNK	c-Jun N-terminal kinases	299.997 nM	Total JNK concentration 300 nM (10)
p-JNK	Monophosphorylated JNK	0.003 nM	---
pp-JNK	Biphosphorylated JNK	0 nM	---
eNOS (mRNAn)	Nuclear eNOS mRNA	0.09 nM	Estimate
eNOS (mRNAc)	Cytosolic eNOS mRNA	3.214 nM	Estimate
eNOS: Cav-1	eNOS (inactive due to Cav-1 binding)	34.98 nM	See model 4

AP-1 (inactive)	Activator Protein-1 (inactive)	50 nM	Total AP-1 concentration 50 nM (estimate)
AP-1 (active)	Activator Protein-1 (active)	0 nM	---
KLF2 (protein)	Krueppel-like factor 2	10 nM	Estimate

*** Initial amounts were obtained by simulating the model under "no flow" condition, with the reference value as initial concentrations, for a sufficient amount of time to reach steady state.**

List of reactions:

#	Description	Rate equation	Ref.
*1	[FAK] ↔ [p-FAK]	$\exp(1-\left(\frac{t}{60}\right)^{0.35})\cdot 4\cdot t^{-0.65}\cdot(1-\left(\frac{t}{60}\right)^{0.35})$	(5)
*2	[Src] ↔ [p-Src]	$\exp(1-\left(\frac{t}{540}\right)^{1.3})\cdot 0.026\cdot t^{0.3}\cdot(1-\left(\frac{t}{540}\right)^{1.3})$	(6)
3	[p-FAK] + [Shc] ↔ [p-FAK:Shc]	$k_3[p-FAK][Shc]-k_{r3}[p-FAK:Shc]$	(8)
4	[p-FAK:Shc] ↔ [p-FAK:p-Shc]	$k_4[p-Src][p-FAK:Shc]-k_{r4}[p-FAK:p-Shc]$	(7, 8)
5	[p-FAK:Shc] + [Grb2:Sos] ↔ [p-FAK:Shc:Grb2:Sos]	$k_5[p-FAK:Shc][Grb2:Sos]-$ $k_{r5}[p-FAK:p-Shc:Grb2:Sos]$	(8)
6	[p-FAK:p-Shc:Grb2:Sos] ↔ [p-FAK] + [p-Shc:Grb2:Sos]	$k_6[p-FAK:p-Shc:Grb2:Sos]-$ $k_{r6}[p-FAK][p-Shc:Grb2:Sos]$	(8)
7	[p-Shc:Grb2:Sos] → [p-Shc] + [Grb2:Sos]	$k_7[p-Shc:Grb2:Sos]$	(8)
8	[p-Shc] → [Shc]	$\frac{V_8[p-Shc]}{K_{m8}+[p-Shc]}$	(8)
9	[Ras:GDP] → [Ras:GTP]	$k_9\frac{[p-Shc:Grb2:Sos][Ras:GTP]}{K_{m9}+[Ras:GTP]}$	(8)
10	[Ras:GTP] → [Ras:GDP]	$\frac{V_{10}[Ras:GTP]}{K_{m10}+[Ras:GTP]}$	(8)
11	[MEKK1] → [p-MEKK1]	$k_{11}\frac{[Ras:GTP][MEKK1]}{K_{m11}+[MEKK1]}$	(10)
12	[p-MEKK1] → [MEKK1]	$\frac{V_{12}[p-MEKK1]}{K_{m12}+[p-MEKK1]}$	(10)
13	[JNKK] → [p-JNKK]	$k_{13}\frac{[p-MEKK1][JNKK]}{K_{m13}+[JNKK]}$	(10)
14	[p-JNKK] → [JNKK]	$\frac{V_{14}[p-JNKK]}{K_{m14}+[p-JNKK]}$	(10)
15	[p-JNKK] → [pp-JNKK]	$k_{15}\frac{[p-MEKK1][p-JNKK]}{K_{m15}+[p-JNKK]}$	(10)
16	[pp-JNKK] → [p-JNKK]	$\frac{V_{16}[pp-JNKK]}{K_{m16}+[pp-JNKK]}$	(10)
17	[JNK] → [p-JNK]	$k_{17}\frac{[pp-JNKK][JNK]}{K_{m17}+[JNK]}$	(10)
18	[p-JNK] → [JNK]	$\frac{V_{18}[p-JNK]}{K_{m18}+[p-JNK]}$	(10)
19	[p-JNK] → [pp-JNK]	$k_{19}\frac{[pp-JNKK][p-JNK]}{K_{m19}+[p-JNK]}$	(10)

20	[pp-JNK] → [p-JNK]	$\frac{V_{20}[pp-JNK]}{K_{m20}+[pp-JNK]}$	(10)
21	[AP-1 (inactive)] → [AP-1 (active)]	$k_{21}\frac{[pp-JNK][AP-1_{(inactive)}]}{K_{m21}+[AP-1_{(inactive)}]}$	Assum.
22	[AP-1 (active)] → [AP-1 (inactive)]	$\frac{V_{22}[AP-1_{(active)}]}{K_{m22}+[AP-1_{(active)}]}$	Assum.
*23	ϕ → [KLF2]	$\frac{\exp(0.55(5-t/3600))/(3600\cdot 29.256)}{(1+2\cdot\exp(0.55(5-t/3600))+\exp(1.1(5-t/3600))}$	(12)
24	ϕ → [eNOS (mRNAn)]	$k_{24t1}[AP-1_{(active)}]+k_{24t2}[KLF2]$	Assum.
25	[eNOS (mRNAn)] → [eNOS (mRNAc)]	$k_{25}[eNOS_{mRNAn}]$	(9)
26	[eNOS (mRNAc)] → ϕ	$k_{26}[eNOS_{mRNAc}]$	(11)
27	ϕ → [eNOS:Cav-1]	$\frac{V_{27}[eNOS_{mRNAc}]}{K_{m27}+[eNOS_{mRNAc}]}$	Assum.

*** Time-dependent functions describing FAK, Src activation, and KLF2 expression were generated from the experimental data in (5, 6, 12). The shear stress waveform used in (5, 6) is a laminar flow of 12 dynes/cm^2, the shear stress waveform used in (12) is an oscillatory (1 Hz) flow of 12±4 dynes/cm^2.**

List of parameters:

	Units	**Ref.**	**Ref. value**	**Model value**
k_3	$nM^{-1} \bullet s^{-1}$	(8)	0.1	0.1
k_{r3}	s^{-1}	(8)	1.0	1.0
k_4	$nM^{-1} \bullet s^{-1}$	(7)	8.33	8.33
k_{r4}	s^{-1}	(8)	5.0	5.0
k_5	$nM^{-1} \bullet s^{-1}$	(8)	60	60
k_{r5}	s^{-1}	(8)	546	546
k_6	s^{-1}	(8)	2040	2040
k_{r6}	$nM^{-1} \bullet s^{-1}$	(8)	15700	15700
k_7	s^{-1}	(8)	40.8	40.8
V_8	$nM \bullet s^{-1}$	(8)	0.0154	154
K_{m8}	nM	(8)	340	340
k_9	s^{-1}	(8)	0.222	0.222
K_{m9}	nM	(8)	0.181	0.181
V_{10}	$nM \bullet s^{-1}$	(8)	0.289	0.289
K_{m10}	nM	(8)	0.0571	0.0571
k_{11}	s^{-1}	Estimated from (10)	---	0.035
K_{m11}	nM	(10)	10	10
V_{12}	$nM \bullet s^{-1}$	(10)	0.25	0.125
K_{m12}	nM	(10)	8.0	8.0
k_{13}	s^{-1}	(10)	0.025	0.005
K_{m13}	nM	(10)	15.0	15.0
V_{14}	$nM \bullet s^{-1}$	(10)	0.75	0.375
K_{m14}	nM	(10)	15.0	15.0
k_{15}	s^{-1}	(10)	0.025	0.005
K_{m15}	nM	(10)	15.0	15.0
V_{16}	$nM \bullet s^{-1}$	(10)	0.75	0.375
K_{m16}	nM	(10)	15.0	15.0
k_{17}	s^{-1}	(10)	0.025	0.002
K_{m17}	nM	(10)	15.0	30.0

V_{18}	nM• s^{-1}	(10)	0.5	0.05
K_{m18}	nM	(10)	15.0	15.0
k_{19}	s^{-1}	(10)	0.025	0.002
K_{m19}	nM	(10)	15.0	30.0
V_{20}	nM• s^{-1}	(10)	0.5	0.05
K_{m20}	nM	(10)	15.0	15.0
k_{21}	s^{-1}	Estimated from fitting exp. data	---	$4.0 * 10^{-5}$
K_{m21}	nM	Estimated from fitting exp. data	---	25.0
V_{22}	nM• s^{-1}	Estimated from fitting exp. data	---	0.002
K_{m22}	nM	Estimated from fitting exp. data	---	5
k_{24t1}	s^{-1}	Estimated from fitting exp. data	---	$1.2 * 10^{-4}$
k_{24t2}	s^{-1}	Estimated from fitting exp. data	---	$9.0 * 10^{-6}$
k_{25}	s^{-1}	(9)	0.001	0.001
k_{26}	s^{-1}	Estimated from (11)	$1.1 * 10^{-5}$	$2.8 * 10^{-5}$
V_{27}	nM• s^{-1}	Estimated from fitting exp. data	---	0.02824
K_{m27}	nM	Estimated from fitting exp. data	---	16

References for model 3:
(5-12)

Model 4: Shear-stress-induced NO production

Model Diagram:

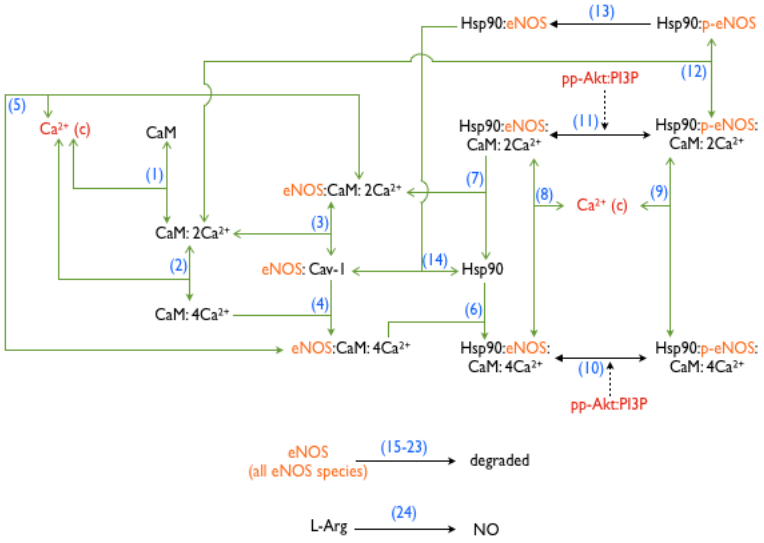

List of species:

Species	**Name**	***Initial Amount**	**Ref.**
Ca^{2+} (c)	Cytosolic calcium	117.2 nM	See Model 1
pp-Akt:PI3P	Biphosphorylated Akt	1.72 nM	See Model 2
CaM	Calmodulin	7635.36 nM	Total CaM concentration 8000 nM (estimate)
CaM:2Ca^{2+}	2 calcium bound calmodulin	347.52 nM	---
CaM:4Ca^{2+}	4 calcium bound calmodulin	2.83 nM	---
eNOS: Cav-1	eNOS (inactive due to Cav-1 binding)	34.98 nM	Total eNOS concentration 50 nM (estimate)
eNOS:CaM:2Ca^{2+}	eNOS protein complex	2.12 nM	---
eNOS:CaM:4Ca^{2+}	eNOS protein complex with calcium/calmodulin-induced activation	0.04 nM	---
Hsp90	Heat shock protein 90	199987 nM	Total Hsp90 concentration 200000 nM (estimate)
Hsp90:eNOS: CaM:2Ca^{2+}	eNOS protein complex	10.98 nM	---
Hsp90:p-eNOS: CaM:2Ca^{2+}	Phosphorylated eNOS protein complex	0.11 nM	---
Hsp90:eNOS: CaM:4Ca^{2+}	eNOS protein complex with calcium/calmodulin-induced activation	1.04 nM	---
Hsp90:p-eNOS: CaM:4Ca^{2+}	Phosphorylated eNOS protein complex with calcium/calmodulin-induced activation	0.01 nM	---
Hsp90:eNOS	eNOS protein complex	0.08 nM	---
Hsp90:p-eNOS	Phosphorylated eNOS protein complex	0.64 nM	---
NO	Nitric Oxide	0 (relative	---

		scale)	

*** Initial amounts were obtained by simulating the model under "no flow" condition, with the reference value as initial concentrations, for a sufficient amount of time to reach steady state.**

List of reactions:

#	Description	Rate equation	*Ref.
1	[CaM] ↔ [CaM:2Ca^{2+}]	$k_1 \cdot [CaM][Ca^{2+}] - k_{1r} \cdot [CaM:2Ca^{2+}]$	Assum.
2	[CaM:2Ca^{2+}] ↔ [CaM:4Ca^{2+}]	$k_2 \cdot [CaM:2Ca^{2+}][Ca^{2+}] - k_{2r} \cdot [CaM:4Ca^{2+}]$	Assum.
3	[CaM:2Ca^{2+}] + [eNOS:Cav-1] ↔ [eNOS:CaM:2Ca^{2+}]	$k_3 \cdot [CaM:2Ca^{2+}][eNOS:Cav-1] - k_{3r} \cdot [eNOS:CaM:2Ca^{2+}]$	Assum.
4	[CaM:4Ca^{2+}] + [eNOS:Cav-1] → [eNOS:CaM:4Ca^{2+}]	$k_4 \cdot [CaM:4Ca^{2+}][eNOS:Cav-1]$	Assum.
5	[eNOS:CaM:4Ca^{2+}] ↔ [eNOS:CaM:2Ca^{2+}]	$k_5 \cdot [eNOS:CaM:4Ca^{2+}] - k_{5r} \cdot [eNOS:CaM:2Ca^{2+}][Ca^{2+}]$	Assum.
6	[eNOS:CaM:4Ca^{2+}] + [Hsp90] → [Hsp90:eNOS:CaM:4Ca^{2+}]	$k_6 \cdot [eNOS:CaM:4Ca^{2+}][Hsp90]$	Assum.
7	[Hsp90:eNOS:CaM:2Ca^{2+}] → [eNOS:CaM:2Ca^{2+}] + [Hsp90]	$k_7 \cdot [Hsp90:eNOS:CaM:2Ca^{2+}]$	Assum.
8	[Hsp90:eNOS:CaM:4Ca^{2+}] ↔ [Hsp90:eNOS:CaM:2Ca^{2+}]	$k_8 \cdot [Hsp90:eNOS:CaM:4Ca^{2+}] - k_{8r} \cdot [Hsp90:eNOS:CaM:2Ca^{2+}][Ca^{2+}]$	Assum.
9	[Hsp90:p-eNOS:CaM:4Ca^{2+}] ↔ [Hsp90:p-eNOS:CaM:2Ca^{2+}]	$k_9 \cdot [Hsp90:p-eNOS:CaM:4Ca^{2+}] - k_{9r} \cdot [Hsp90:p-eNOS:CaM:2Ca^{2+}][Ca^{2+}]$	Assum.
10	[Hsp90:eNOS:CaM:4Ca^{2+}] ↔ [Hsp90:p-eNOS:CaM:4Ca^{2+}]	$\frac{k_{10}[pp-AKT:PI3P][Hsp90:eNOS:CaM:4Ca^{2+}]}{K_{m10}+[Hsp90:eNOS:CaM:4Ca^{2+}]} - \frac{V_{10r}[Hsp90:p-eNOS:CaM:4Ca^{2+}]}{K_{m10r}+[Hsp90:p-eNOS:CaM:4Ca^{2+}]}$	Assum.
11	[Hsp90:eNOS:CaM:2Ca^{2+}] ↔ [Hsp90:p-eNOS:CaM:2Ca^{2+}]	$\frac{k_{11}[pp-AKT:PI3P][Hsp90:eNOS:CaM:2Ca^{2+}]}{K_{m11}+[Hsp90:eNOS:CaM:2Ca^{2+}]} - \frac{V_{11r}[Hsp90:p-eNOS:CaM:2Ca^{2+}]}{K_{m11r}+[Hsp90:p-eNOS:CaM:2Ca^{2+}]}$	Assum.
12	[Hsp90:p-eNOS:CaM:2Ca^{2+}] ↔ [Hsp90:p-eNOS] + [CaM:2Ca^{2+}]	$k_{12} \cdot [Hsp90:p-eNOS:CaM:2Ca^{2+}] - k_{12r} \cdot [Hsp90:p-eNOS][CaM:2Ca^{2+}]$	Assum.
13	[Hsp90:p-eNOS] → [Hsp90: eNOS]	$\frac{V_{13}[Hsp90:p-eNOS]}{K_{m13}+[Hsp90:p-eNOS]}$	Assum.
14	[Hsp90:eNOS] → [Hsp90] + [eNOS:Cav-1]	$k_{14} \cdot [Hsp90:eNOS]$	Assum.
15	[eNOS:Cav-1] → ϕ	$k_D \cdot [eNOS:Cav-1]$	Assum.
16	[eNOS:CaM:2Ca^{2+}] → ϕ + [CaM:2Ca^{2+}]	$k_D \cdot [eNOS:CaM:2Ca^{2+}]$	Assum.
17	[eNOS:CaM:4Ca^{2+}] → ϕ + [CaM:4Ca^{2+}]	$k_D \cdot [eNOS:CaM:4Ca^{2+}]$	Assum.
18	[Hsp90:eNOS:CaM:2Ca^{2+}] → ϕ + [CaM:2Ca^{2+}] + [Hsp90]	$k_D \cdot [Hsp90:eNOS:CaM:2Ca^{2+}]$	Assum.
19	[Hsp90:eNOS:CaM:4Ca^{2+}] → ϕ + [CaM:4Ca^{2+}] + [Hsp90]	$k_D \cdot [Hsp90:eNOS:CaM:4Ca^{2+}]$	Assum.
20	[Hsp90:p-eNOS:CaM:2Ca^{2+}] → ϕ + [CaM:2Ca^{2+}] + [Hsp90]	$k_D \cdot [Hsp90:p-eNOS:CaM:2Ca^{2+}]$	Assum.
21	[Hsp90:p-eNOS:CaM:4Ca^{2+}] → ϕ + [CaM:4Ca^{2+}] + [Hsp90]	$k_D \cdot [Hsp90:p-eNOS:CaM:4Ca^{2+}]$	Assum.
22	[Hsp90:p-eNOS] → ϕ + [Hsp90]	$k_D \cdot [Hsp90:p-eNOS]$	Assum.

23	[Hsp90:eNOS] $\rightarrow \phi$ + [Hsp90]	$k_D \cdot [Hsp90:eNOS]$	Assum.
24	$\phi \rightarrow$ [NO]	$k_{CaM} \cdot [Hsp90:eNOS:CaM:4Ca^{2+}] +$ $k_{CaM} \cdot [Hsp90:p-eNOS:CaM:4Ca^{2+}] +$ $k_{CaM} \cdot [eNOS:CaM:4Ca^{2+}] +$ $k_p \cdot [Hsp90:p-eNOS:CaM:2Ca^{2+}] +$ $k_p \cdot [Hsp90:p-eNOS]$	Assum.

*** All reactions from this model were generated based on our assumptions.**

List of parameters:

	Units	**Ref.**	**Ref. value**	**Model value**
k_1	$nM^{-1} \bullet s^{-1}$	Estimated from (13)	---	0.004
k_{1r}	s^{-1}	Estimated from (13)	---	10.3
k_2	$nM^{-1} \bullet s^{-1}$	Estimated from (13)	---	0.08
k_{2r}	s^{-1}	Estimated from (13)	---	1152
k_3	$nM^{-1} \bullet s^{-1}$	Initial estimate	---	$1.5 * 10^{-4}$
k_{3r}	s^{-1}	Initial estimate	---	1.5
k_4	$nM^{-1} \bullet s^{-1}$	Initial estimate	---	0.015
k_5	s^{-1}	Estimated from (13)	---	115.2
k_{5r}	$nM^{-1} \bullet s^{-1}$	Estimated from (13)	---	0.08
k_6	$nM^{-1} \bullet s^{-1}$	Estimated from (15)	---	0.002
k_7	s^{-1}	Estimated from (15)	---	1.5
k_8	s^{-1}	Estimated from (13)	---	115.2
k_{8r}	$nM^{-1} \bullet s^{-1}$	Estimated from (13)	---	0.08
k_9	s^{-1}	Estimated from (13)	---	115.2
k_{9r}	$nM^{-1} \bullet s^{-1}$	Estimated from (13)	---	0.08
k_{10}	s^{-1}	Estimated from fitting exp. data	---	0.1
K_{m10}	nM	Estimated from fitting exp. data	---	5
V_{10r}	$nM \bullet s^{-1}$	Estimated from fitting exp. data	---	4
K_{m10r}	nM	Estimated from fitting exp. data	---	20
k_{11}	s^{-1}	Estimated from fitting exp. data	---	0.1
K_{m11}	nM	Estimated from fitting exp. data	---	5
V_{11r}	$nM \bullet s^{-1}$	Estimated from fitting exp. data	---	4
K_{m11r}	nM	Estimated from fitting exp. data	---	20
k_{12}	s^{-1}	Initial estimate	---	1.5
k_{12r}	$nM^{-1} \bullet s^{-1}$	Initial estimate	---	$1.5 * 10^{-4}$
V_{13}	$nM \bullet s^{-1}$	Estimated from fitting exp. data	---	4
K_{m13}	nM	Estimated from fitting exp. data	---	20
k_{14}	s^{-1}	Estimated from (15)	---	1.5
k_D	s^{-1}	Estimated from half life (16)	$1.13 * 10^{-5}$	$9.45 * 10^{-5}$
k_{CaM}	s^{-1}	Estimated from (14)	---	17
k_p	s^{-1}	Estimated from (14)	---	5

References for model 4:
(13-16)

Time-dependent functions as model inputs

As described in the manuscript, time-dependent functions were used as model inputs throughout the NO systems as proxies for the mechanotransduction process. These time-dependent functions were either taken directly from existing models or fit from experimental data. The details of the five time-dependent functions are described below:

1) Production of IP3 (Model 1: Reaction 3)

$$\frac{d[IP3]}{dt} = k_1 \cdot (R_T - \frac{R_T}{2} \cdot (e^{-t/\tau_I} + e^{-t/\tau_{II}}) + \left(\frac{\tau_I + \tau_{II}}{\tau_I - \tau_{II}}\right) \cdot (e^{-t/\tau_I} - e^{-t/\tau_{II}})) \cdot \left(\frac{[Ca^{2+}(c)]}{K_1 + [Ca^{2+}(c)]}\right)$$

This equation was taken directly from the calcium dynamics model created by Wiesner et al. (1) through combining *Eq. 11* and *Eq. 16* of the original paper. This theoretical model was based on experimental measurement of human umbilical vein endothelial cells (HUVECs) assuming a laminar shear stress of 10 dynes/cm^2.

2) PI3K Activation (Model 2: Reaction 1)

The equation describing PI3K activation was generated by fitting the experimental data of Go et al. (4) (Figure 2B of the paper) to the following equation:

$$[p-PI3K]_t = 1 + a \cdot \left(\frac{t}{b}\right)^c \cdot \exp(1 - \left(\frac{t}{b}\right)^c)$$

Parameter values of a, b, c were optimized by curve-fitting using MATLAB. We then calculated the time-derivative of the above equation to obtain the time-dependent differential equation of PI3K activation (as shown in Model 2: Reaction 1):

$$\frac{d[p-PI3K]}{dt} = \exp(1 - \left(\frac{t}{15}\right)^{1.8}) \cdot 0.907 \cdot t^{0.8} \cdot (1 - \left(\frac{t}{15}\right)^{1.8})$$

In the Go et al. study, bovine aortic endothelial cells (BAECs) were exposed to a laminar shear stress of 5 dynes/cm^2. PI3K in the time-course experiments was isolated through immunoprecipitation and the PI3K activity was measured by a radioactive assay. Total PI3K concentration was assumed to be 100 nM based on the model of Koh et al. (3).

3) FAK Activation (Model 3: Reaction 1)

Similarly, the equation describing FAK activation was generated by fitting the experimental data of Li et al. (5) (Figure 2A of the paper) to the following equation:

$$[p-FAK]_t = 1 + a \cdot \left(\frac{t}{b}\right)^c \cdot \exp(1 - \left(\frac{t}{b}\right)^c)$$

Parameter values of a, b, c were optimized by curve-fitting using MATLAB. We then calculated the time-derivative of the above equation to obtain the time-dependent differential equation of FAK activation (as shown in Model 3: Reaction 1):

$$\frac{d[p-FAK]}{dt} = \exp(1 - \left(\frac{t}{60}\right)^{0.35}) \cdot 4 \cdot t^{-0.65} \cdot (1 - \left(\frac{t}{60}\right)^{0.35})$$

In the Li et al. study, BAECs were exposed to a laminar shear stress of 12 dynes/cm^2. FAK in the time-course experiments was isolated through immunoprecipitation and FAK activation was measured using a phophotyrosine-specific antibody. Total FAK concentration was assumed to be 80 nM based on the model of Yee et al. (7).

4) Src Activation (Model 3: Reaction 2)

Again, the equation describing Src activation was generated by fitting the experimental data of Jalali et al. (6) (Figure 1 of the paper) to the following equation:

$$[p-Src]_t = 1 + a \cdot \left(\frac{t}{b}\right)^c \cdot \exp\left(1 - \left(\frac{t}{b}\right)^c\right)$$

Parameter values of a, b, c were optimized by curve-fitting using MATLAB. We then calculated the time-derivative of the above equation to obtain the time-dependent differential equation of Src activation (as shown in Model 3: Reaction 2):

$$\frac{d[p-Src]}{dt} = \exp\left(1 - \left(\frac{t}{540}\right)^{1.3}\right) \cdot 0.026 \cdot t^{0.3} \cdot \left(1 - \left(\frac{t}{540}\right)^{1.3}\right)$$

In the Jalali et al. study, BAECs were exposed to a laminar shear stress of 12 dynes/cm^2. Src in the time-course experiment was isolated through immunoprecipitation and the Src activity was measured by a radioactive assay. Total Src concentration was assumed to be 90 nM based on the model of Yee et al. (7).

5) KLF2 Activation (Model 3: Reaction 23)

The equation describing KLF2 activation was generated by fitting the experimental data of Young et al. (12) (Figure 1B of the paper, assuming the translational process is fast and KLF2 protein expression corresponds well with mRNA expression) to the following equation (t/3600 to adjust the time from hours to seconds):

$$[KLF2]_t = 1 + \frac{a}{1 + \exp\left(b \cdot \left(c - \frac{t}{3600}\right)\right)}$$

Parameter values of a, b, c were optimized by curve-fitting using MATLAB. We then calculated the time-derivative of the above equation to obtain the time-dependent differential equation of KLF2 activation (as shown in Model 3: Reaction 23):

$$\frac{d[KLF2]}{dt} = \frac{\exp\left(0.55\left(5 - \left(\frac{t}{3600}\right)\right)\right)/(3600 * 29.256)}{\left(1 + 2 \cdot \exp\left(0.55\left(5 - \left(\frac{t}{3600}\right)\right)\right) + \exp\left(1.1\left(5 - \left(\frac{t}{3600}\right)\right)\right)\right)}$$

In the Young et al. study, HUVECs were exposed to an oscillatory (1 Hz) shear stress of 12±4 dynes/cm^2. mRNA from endothelial cells was isolated in the time-course experiments and relative mRNA expression was measured through qPCR. Initial KLF2 concentration was assumed to be 10 nM based on our experimental observation of low quantity presence in endothelial cells.

Parameter Optimization

The parameters of individual models were optimized in CellDesigner based on the following general iterative steps:

1. Conduct parameter sensitivity analysis to search for the high sensitive parameters (Simulation -> Control Panel -> Interactive Simulation -> Parameter Value).
2. Optimize the set of most sensitive parameters to fit the experimental observed values.

Model 1: Shear stress-induced calcium influx

It is observed through parameter scan that most kinetic parameters that govern reaction rates in this model (k_1, k_2, k_3, k_4, k_5, k_6, k_7, Q_{shear}, V_P, V_{ex}, V_{hi}, τ_I, τ_{II}) need to be adjusted simultaneously in order to achieve sensible simulation outcome. The experimental data used to optimize the parameters is from the study of Schwarz *et al.* (17).

Model 2: Shear stress-induced AKT phosphorylation

The parameters k_2 and k_3 were found to be the most sensitive parameters. These parameters were moderately optimized within the same order of magnitude to better fit the experimental data of Boo *et al.* (18).

Model 3: Shear stress-induced eNOS expression

There was a big shift in V_8 due to modification of model structure compared to the reference model. Other parameters (including the eNOS degradation parameter k_D listed in the 4th model) were estimated or moderately optimized within the same order of magnitude to better fit the experimental data of our lab (eNOS mRNA time course) and the study of Li *et al.* (19) (eNOS protein time course).

Model 4: Shear stress-induced NO production

Most of the parameters in this model are direct estimation from experimental data without further optimization. The parameters governing eNOS phosphorylation (reaction 10 and 11) and dephosphorylation (reaction 13) were optimized according to eNOS phosphorylation time course data from Boo *et al.* (18). The two NO production parameters, k_{CaM} and k_p, were optimized to better fit the experimental observation of Florian *et al.* (20) under both static and shear stress conditions.

Model diagram legends:

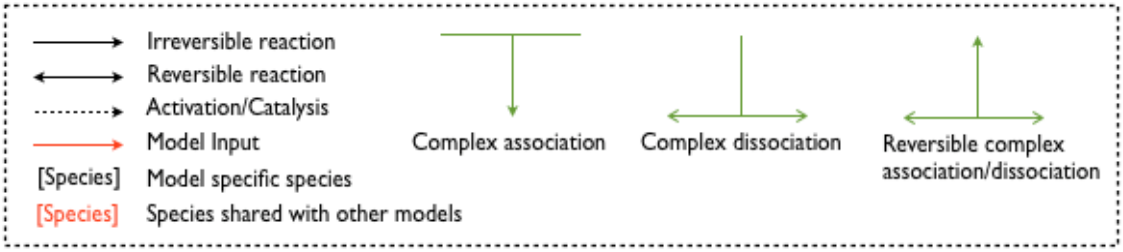

SUPPORTING REFERENCES

1. Wiesner, T. F., B. C. Berk, and R. M. Nerem. 1996. A mathematical model of cytosolic calcium dynamics in human umbilical vein endothelial cells. Am J Physiol 270:C1556-1569.
2. Wiesner, T. F., B. C. Berk, and R. M. Nerem. 1997. A mathematical model of the cytosolic-free calcium response in endothelial cells to fluid shear stress. Proc Natl Acad Sci USA 94:3726-3731.
3. Koh, G., H. F. C. Teong, M.-V. Clément, D. Hsu, and P. S. Thiagarajan. 2006. A decompositional approach to parameter estimation in pathway modeling: a case study of the Akt and MAPK pathways and their crosstalk. Bioinformatics 22:e271-280.
4. Go, Y. M., H. Park, M. C. Maland, V. M. Darley-Usmar, B. Stoyanov, R. Wetzker, and H. Jo. 1998. Phosphatidylinositol 3-kinase gamma mediates shear stress-dependent activation of JNK in endothelial cells. Am J Physiol 275:H1898-1904.
5. Li, S., M. Kim, Y. L. Hu, S. Jalali, D. D. Schlaepfer, T. Hunter, S. Chien, and J. Y. Shyy. 1997. Fluid shear stress activation of focal adhesion kinase. Linking to mitogen-activated protein kinases. J Biol Chem 272:30455-30462.
6. Jalali, S., Y. S. Li, M. Sotoudeh, S. Yuan, S. Li, S. Chien, and J. Y. Shyy. 1998. Shear stress activates p60src-Ras-MAPK signaling pathways in vascular endothelial cells. Arterioscler Thromb Vasc Biol 18:227-234.
7. Yee, K. L., V. M. Weaver, and D. A. Hammer. 2008. Integrin-mediated signalling through the MAP-kinase pathway. IET Syst Biol 2:8-15.
8. Hatakeyama, M., S. Kimura, T. Naka, T. Kawasaki, N. Yumoto, M. Ichikawa, J. H. Kim, K. Saito, M. Saeki, M. Shirouzu, S. Yokoyama, and A. Konagaya. 2003. A computational model on the modulation of mitogen-activated protein kinase (MAPK) and Akt pathways in heregulin-induced ErbB signalling. Biochem J 373:451-463.
9. Yamada, S., S. Shiono, A. Joo, and A. Yoshimura. 2003. Control mechanism of JAK/STAT signal transduction pathway. FEBS Lett 534:190-196.
10. Kholodenko, B. N. 2000. Negative feedback and ultrasensitivity can bring about oscillations in the mitogen-activated protein kinase cascades. Eur J Biochem 267:1583-1588.
11. Weber, M., C. H. Hagedorn, D. G. Harrison, and C. D. Searles. 2005. Laminar shear stress and 3' polyadenylation of eNOS mRNA. Circ Res 96:1161-1168.
12. Young, A., W. Wu, W. Sun, H. Benjamin Larman, N. Wang, Y. S. Li, J. Y. Shyy, S. Chien, and G. Garcia-Cardena. 2009. Flow activation of AMP-activated protein kinase in vascular endothelium leads to Kruppel-like factor 2 expression. Arterioscler Thromb Vasc Biol 29:1902-1908.
13. Black, D. J., J. Leonard, and A. Persechini. 2006. Biphasic Ca2+-dependent switching in a calmodulin-IQ domain complex. Biochemistry 45:6987-6995.
14. Kuchan, M. J., and J. A. Frangos. 1994. Role of calcium and calmodulin in flow-induced nitric oxide production in endothelial cells. Am J Physiol 266:C628-636.
15. Garcia-Cardena, G., R. Fan, V. Shah, R. Sorrentino, G. Cirino, A. Papapetropoulos, and W. C. Sessa. 1998. Dynamic activation of endothelial nitric oxide synthase by Hsp90. Nature 392:821-824.
16. Liu, J., G. Garcia-Cardena, and W. C. Sessa. 1995. Biosynthesis and palmitoylation of endothelial nitric oxide synthase: mutagenesis of palmitoylation sites, cysteines-15 and/or -26, argues against depalmitoylation-induced translocation of the enzyme. Biochemistry 34:12333-12340.
17. Schwarz, G., G. Callewaert, G. Droogmans, and B. Nilius. 1992. Shear stress-induced calcium transients in endothelial cells from human umbilical cord veins. J Physiol 458:527-538.
18. Boo, Y. C., G. Sorescu, N. Boyd, I. Shiojima, K. Walsh, J. Du, and H. Jo. 2002. Shear stress stimulates phosphorylation of endothelial nitric-oxide synthase at Ser1179 by Akt-independent mechanisms: role of protein kinase A. J Biol Chem 277:3388-3396.
19. Li, Y., J. Zheng, I. M. Bird, and R. R. Magness. 2005. Effects of pulsatile shear stress on signaling mechanisms controlling nitric oxide production, endothelial nitric oxide synthase phosphorylation, and expression in ovine fetoplacental artery endothelial cells. Endothelium 12:21-39.
20. Florian, J. A., J. R. Kosky, K. Ainslie, Z. Pang, R. O. Dull, and J. M. Tarbell. 2003. Heparan sulfate proteoglycan is a mechanosensor on endothelial cells. Circ Res 93:e136-142.